DEGREE PROJECT IN TECHNOLOGY,
FIRST CYCLE, 15 CREDITS
STOCKHOLM, SWEDEN 2018

On development lengths of Asymptotic Suction Boundary Layers

JORGE ARNEDO GARCÍA

KTH ROYAL INSTITUTE OF TECHNOLOGY
SCHOOL OF ENGINEERING SCIENCES

EXAMENSARBETE INOM TEKNIK,
GRUNDNIVÅ, 15 HP

STOCKHOLM, *SVERIGE 2018*

På utvecklingslängder av Asymptotisk sugning Gränslag

JORGE ARNEDO GARCÍA

KTH
SKOLAN FÖR TEKNIKVETENSKAP

ABSTRACT

The application of suction in order to control the boundary-layer behaviour can be a major advancement in aerospace technology. In this thesis the asymptotic state of the suction boundary-layer is studied in depth, as well as the different developments that such boundary layers can have in space and in time. The final goal of the thesis is to estimate a numerical parameter that relates space and time which would help to calculate the required streamwise length that a wind tunnel should have to reach the asymptotic state of the suction boundary layer. The study is done by means of computational simulations of flows (CFD) and more concretely Direct Numerical Simulations (DNS). The simulations are done with the KTH Software SIMSON which was developed with the purpose of study boundary-layer flows. All the data generated by the simulations was postprocessed using MATLAB.

SAMMANFATTNING

Tillämpningen av sug för att styra gränsskiktets beteende kan vara en stor framsteg inom flygteknik. I denna avhandling studeras det asymptotiska tillståndet av suggränsskiktet i djupet, liksom den olika utveckling som sådana gränsvärden kan ha i rymden och i tiden. Avhandlingens slutmål är att uppskatta en numerisk parameter som avser utrymme och tid som skulle bidra till att beräkna den önskade strömlängden att en vindtunnel skulle behöva nå det asymptotiska tillståndet hos suggränskiktet. Studien görs med hjälp av beräkningssimuleringar av flöden, CFD och mer konkreta direkta numeriska simuleringar (DNS). Simuleringarna görs med KTH Software SIMSON som utvecklades med syftet att studera gränsskiktflöden. Alla data som genererades av simuleringarna efterbehandlades med MATLAB.

ACKNOWLEDGEMENTS

I would like to express my gratitude, first of all, to Ricardo Vinuesa who has been my main guide regarding this project. He has shown me a first glance of the research world and I will always be grateful for that. I would also like to thank the help provided by Philipp Schlatter who solved me many doubts about the project. Finally, I would like to thank my parents for giving me the possibility of doing my Bachelor Thesis at KTH and also for being a continuous source of inspiration and support.

The numerical simulations have been carried out on resources provided by the Mechanics Department of KTH.

CONTENTS

LIST OF FIGURES

LIST OF TABLES

1 | INTRODUCTION

1.1 MOTIVATION

Since its birth at the very beginning of the last century, aviation has always been linked to technology breakthroughs and subjected to continuous improvement. It is one of the most demanding fields as a consequence of the numerous constraints such as the weight and it requires to take into account every single detail, even the smaller ones. A well-known example of that is the case of the drag, where a change in the third decimal of the drag coefficient can be vital.

Drag reduction has always been a major issue for aircraft designers due to its possible positive outcomes: reduced fuel consumption, larger operational range, greater endurance and higher achievable speeds. There are two main sources of drag: skin-friction drag and lift-induced drag. While the second one is caused by the wingtip vortices which induce an increased angle of attack and occurs only when lift is generated, the first one is almost entirely related to the state of the boundary layer [7]. Then, having a deep understanding of the boundary layer development is crucial for being able to control the flow.

There are a wide range of methods in order to reduce the friction drag. One possibility consists on reducing the turbulent friction by manipulating the turbulent boundary layer using devices as “riblets" and “Large Eddy Break-Up" which limit the appearance of large eddys, the greatest source of turbulent drag. However, this first method only can accomplish a 5-15 % of drag reduction as the boundary layer is already turbulent. Another method consists on maintain the laminar boundary layer by means of applying suction on particular areas of the wing. This method can achieve a 50-80 % of drag reduction thanks to the delayed transition of the laminar boundary layer. In addition, suction can be employed to delay the separation or stabilize the flow over the wing.

In the last paragraph, the importance of suction in the aeronautics field was proven. Despite that, the real implementation of suction in aircraft has been difficult due to technical aspects and also due to the fact that the data available corresponding to suction boundary layers, both experimental and numerical, are within the domain of much lower Reynolds numbers than those experienced during flight. As a consequence, there exists a necessity of understanding the suction boundary layer in depth and widen the data base available. Once its understanding is complete, its application will be easier, more efficient and not only in the aeronautical field. The flow control by means of suction has other possible relevant applications such as the reduction of pumping power in pipes associated to prevent the transition to turbulent flow [8].

The main purpose of this thesis is to give a general view of the steady state of the suction boundary layer, the asymptotic state, from the perspective of direct numerical simulations (DNS). In addition, it intends to study how the suction boundary layer develops spatially and how is this spatial development related to the temporal one.

1.2 BACKGROUND

Although this topic can seem to be relatively new, the fact is that was Ludwig Prandtl who first mentioned the suction boundary layer. It was in his article of 1904 where he developed the concept of boundary layer using the Navier–Stokes equations and at the same time he suggested different ways to possibly control it [9].

Years after that, Schlichting found out that there existed a special case of suction where the boundary-layer thickness δ_{99} remained constant along the streamwise direction after a certain period in which the growth of the boundary-layer was slowly diminished [1]. This state was called asymptotic suction boundary-layer (ASBL). Griffith and Meredith were the first ones to formulate an analytical approach to the laminar state of the ASBL [10] while years later, Kay was the first researcher to obtain the laminar asymptotic state through experiments [11]. It was not until ten years after that the turbulent asymptotic suction boundary layer was firstly shown experimentally by Dutton [12]. However, a general asymptotic solution was not possible to find, so the asymptotic turbulent state was only proven for a critical suction. In the early 1970s, Rotta was able to derive a description of the turbulent case using Prandtl's mixing length theory and also to corroborate it through experiments [13].

In 1993, Mariani et al. [14] conducted the first direct numerical simulation of the turbulent suction boundary layer opening the door to a great number of numerical results on the ASBL, although a general asymptotic state for the turbulent case has not yet achieved. There is also a lack of agreement on how to scale the mean velocity profile, using a logarithmic or a bi-logarithmic law.

This thesis will continuously make reference to two articles from the last years, Bobke et al. [3] and Ferro et al. [15] as they provide data of good accuracy. The first one gives a numerical perspective of the TASBL stating that an asymptotic state is not achievable in a realistic facility due to the length required to reach it, while the second one, from an experimental point of view, claims that reaching an asymptotic state is possible backed up by the results obtained.

1.3 STRUCTURE

In order to understand the scope of this thesis it is important to have a general view of its content. As one of the main goals is to gain a substantial knowledge about

the asymptotic suction boundary layer, the thesis must be structured consequently by introducing the concepts slowly. The first chapter intends to give a general view of the concept of boundary layer giving some examples and introducing its formulation. The second one is more focused on the method used to do the thesis, DNS, so the simulation set-up is introduced. After that, the results are exposed, separating between chapters the laminar and the turbulent cases. While the laminar chapter is introduced by the theoretical analysis of the ASBL, the turbulent one is introduced with a brief description of what turbulence is and how it is treated. Both results chapters are subdivided to show on one side the temporal simulations and on the other the spatial ones, to finally compare them. A brief conclusion is included at the end of the thesis to summarize the results.

2 BOUNDARY-LAYER THEORY

In order to achieve a deep understanding on asymptotic suction boundary layers it is important to perfectly understand the very basics of the general boundary-layer theory. Therefore, the goal of this chapter is to give a global view of the theory behind the concept of boundary layer.

2.1 FLUID MECHANICS FUNDAMENTALS

The study of fluid behaviour is as old as our civilisation. It was at the Ancient Greece where the first development of this field occurred by the hand of Archimedes, who established the fundamental principles of hydrodynamics. However, it was not until the appearance of Sir Isaac Newton that the knowledge of fluid flow can be considered a science. He investigated particularly the shear stress between layers of fluid establishing a linear relation between it and the velocity of the flow. In his work Philosophiae Naturalis Principia Mathematica (1687) he formulates the three laws of movement or "the three Newton's laws" which, together with the differential calculus, also developed by Newton, were the key for further development of the fluid mechanics field and for the science in general.

After Newton's work many problems were solved and a lot of scientist and mathematicians continued to developed fluid mechanics. Bernoulli proved that the changes of pressure are proportional to the changes of velocity in fluids, although his principle was not general. Euler solved the question of fluids in motion with his partial differential equations, the first time that the flow was expressed using differentials. However, it was not until the 1840's when Navier and Stokes, simultaneously, added the viscosity term to the Euler equations, generating the very well-known Navier–Stokes equations. Together with the turbulence theory initiated by Reynolds years later, they are the cornerstone of modern fluid mechanics.

In order to describe a flow by means of governing equations in the most general way, it is needed to use the conservation laws. There are three magnitudes that are conserved when analysing a flow from a control volume point of view based on the eulerian approach: mass (eq. 2.1), momentum (eq. 2.2) and energy (eq. 2.3). The formulation of the conservation of mass is called continuity equation and states that the rate at which mass enter the control volume is the same at which mass leaves it. The conservation of momentum is a result derived from the Second Newton's Law and when applied to a control volume needs the inclusion of surface forces, pressure

and friction. There are three conservation of momentum equations, one per direction, and the three of them conform the Navier–Stokes equations. Finally, conservation of energy equation is a reformulation of the First Law of Thermodynamics adapted to control volumes.

$$\frac{\partial \rho}{\partial t} + \frac{\partial}{\partial x_i}(u_i \rho) = 0 \tag{2.1}$$

$$\rho\left(\frac{\partial u_i}{\partial t} + u_j \frac{\partial u_i}{\partial x_j}\right) = -\frac{\partial P}{\partial x_i} + \frac{\partial}{\partial x_j}\left[\mu\left(\frac{u_i}{x_j} + \frac{u_j}{x_i}\right)\right] - \frac{2}{3}\mu\frac{\partial}{\partial x_i}\left(\frac{\partial u_k}{x_k}\right) + \rho F_i \tag{2.2}$$

$$\rho\left(\frac{\partial E}{\partial t} + u_i \frac{\partial E}{\partial x_i}\right) = -P\frac{\partial u_i}{\partial x_i} + \mu\frac{\partial u_i}{\partial x_j}\left(\frac{\partial u_i}{\partial x_j} + \frac{\partial u_j}{\partial x_i} - \frac{2}{3}\frac{\partial u_k}{x_k}\delta_{ij}\right) + \frac{\partial}{\partial x_i}\left(\kappa\frac{\partial T}{\partial x_i}\right) \tag{2.3}$$

Looking above is possible to distinguish five different equations: 1 continuity equation, 3 momentum conservation equations and 1 energy conservation equation; while there are six unknowns: the three components of velocity, density, pressure and temperature. Therefore, there exist a closure problems. In order to solve it, an equation of state relating density, pressure and temperature and a thermodynamic equation, relating energy with temperature must be added to the set of equations. If ,for example, the fluid is a perfect gas, the equation of state would be $p = \rho RT$.

The resulting set of equations is extremely hard to solve in practice as they are coupled. This means that it is impossible to solve a single equation without solving all the others. Therefore, it is necessary to make some simplifications in order to be able to work with them. A very common simplification when dealing with boundary layers is to assume that the flow is incompressible. Making this assumption implies that the fluid particle experiences no change in volume, so the density is constant $\rho = cnst \rightarrow \frac{\partial \rho}{\partial t} = 0$. Assuming incompressibility has another major implication, it decouples the energy equation which means that it is possible to solve the mass and momentum equation together without solving the energy one. This assumption is only valid when there are no large pressure changes, situation that can be evaluated using the Mach number. If $Ma < 0.3$ then the flow can be considered incompressible.

After applying the mentioned assumptions, the set of equations is reduced to these, the Incompressible Navier-Stokes equations:

$$\frac{\partial u_i}{\partial x_i} = 0 \tag{2.4}$$

$$\frac{\partial u_i}{\partial t} + u_j \frac{\partial u_i}{\partial x_j} = -\frac{1}{\rho}\frac{\partial P}{\partial x_i} + \nu\nabla^2 u_i + F_i \tag{2.5}$$

2.2 BOUNDARY-LAYER CONCEPT

At the end of the 19th century there was a great misunderstanding between the theorists and the experimentalists of the fluid mechanics field, the experiments were not confirming the theoretical results. The main cause of that was the fact that theorists were using the Euler equations to model the flow behaviours, which means that they were assuming that the fluid was inviscid, null viscosity, or, in other words, the Reynolds number was big $Re = \frac{U_\infty L}{\nu} \to \infty$. Although they knew the Navier–Stokes equations for half a century, their mathematical complexity made them not very useful for practical situations. In addition to that, for technical useful fluids such as water or air, the viscous forces were negligible compared to gravity and pressure forces. The problem of neglecting viscosity was that the no-slip condition was not fulfilled so the flow was badly modelled. The Euler equations were unable to predict the drag of a body immersed in a fluid, fact that supposed a great challenge at that moment.

It was Ludwig Prandtl in 1904 in his lecture "Über Flüssigkeitbewegung bei sehr kleiner Reibung" (On Fluid Motion with Very Small Friction) who solved the drag's problem and, at the same time, he was able to reconcile the experiments with the theory. His idea consisted on dividing the flow into two regions: a very thin layer close to the wall where the effects of viscosity are significant, and the remaining region outside this thin layer where viscosity can be neglected. The inner thin layer was called boundary layer and solved the problem of the no-slip condition as inside it the flow developed from the 0 speed at the wall to almost the bulk velocity. The mathematical complexity implied in the viscous flows was considerably reduced as they were able to treat the boundary layer separately from the bulk flow, which could be considered inviscid. The drag's problem was solved and a considerably stimulation of the fluid mechanics field was given by Prandtl [1].

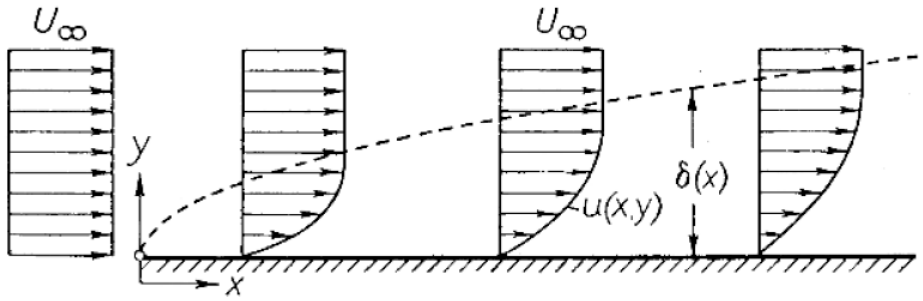

Figure 1: Boundary-layer velocity profile close to an impermeable wall [1]

2.3 BOUNDARY-LAYER EQUATIONS

In order to obtain the equations that control the behaviour of the flow inside the boundary layer, it is better to use the 2D case shown by figure 1 although the 3D case is analogous. Then, it can be assumed that $\frac{\partial}{\partial z} = 0$. It is also assumed that there are no external forces ($F_i = 0$). The method used to obtain the equations consists on a dimensional analysis of the incompressible Navier–Stokes equations taking into account the mentioned simplifications above. To do that it is important to firstly state the dimension of all the variables involved:

L	length scale for	x
δ	length scale for	y
U_0	velocity scale for	u
α	velocity scale for	v
ρ_0	density scale for	ρ
$\frac{L}{U_0}$	time scale for	t
$\rho_0 U_0^2$	pressure scale for	P
ν_0	viscosity scale for	ν

Applying the dimensional analysis to the continuity equation where $\mathcal{O}$ makes reference to the order of magnitude

$$\frac{\partial u}{\partial x} + \frac{\partial v}{\partial y} = 0$$
$$\mathcal{O}\left(\frac{U_0}{L}\right) + \mathcal{O}\left(\frac{\alpha}{\delta}\right) = 0$$

That implies:

$$\frac{U_0}{L} \sim \frac{\alpha}{\delta} \rightarrow \alpha \sim U_0 \frac{\delta}{L}$$

The same analysis must be applied to the momentum conservation equations. Firstly, the momentum equation in the vertical direction is given by:

$$\begin{array}{ccccccccc}
\frac{\partial v}{\partial t} & + & u\frac{\partial v}{\partial x} & + & v\frac{\partial v}{\partial y} & = & -\frac{1}{\rho}\frac{\partial P}{\partial y} & + & \nu\frac{\partial^2 v}{\partial x^2} & + & \nu\frac{\partial^2 v}{\partial y^2} \\
\frac{\delta U_0}{L}\frac{U_0}{L} & & U_0\frac{1}{L}\frac{\delta U_0}{L} & & \frac{\delta U_0}{L}\frac{1}{\delta}\frac{\delta U_0}{L} & & \frac{1}{\rho_0}\frac{\rho_0 U_0^2}{\delta} & & \frac{\nu_0}{L^2}\frac{\delta U_0}{L} & & \frac{\nu_0}{\delta^2}\frac{\delta U_0}{L} \\
\left(\frac{\delta}{L}\right)^2 & & \left(\frac{\delta}{L}\right)^2 & & \left(\frac{\delta}{L}\right)^2 & & 1 & & \frac{1}{Re}\left(\frac{\delta}{L}\right)^2 & & \frac{1}{Re}
\end{array}$$

The third row is the result of multiplying the second row by $\frac{\delta}{U_0^2}$, while the second row just represents the dimensions of the y-momentum equation. As it is being considered that the Reynolds number is very big $Re \to \infty$ and that the boundary-layer thickness is negligible compared with the characteristic dimension in x, then $L >>> \delta \to \left(\frac{\delta}{L}\right)^2 <<< 1$. Therefore, the pressure term is the only one that is of first order $\mathcal{O}(1)$, which means that the pressure do not change through the boundary-layer thickness in the vertical coordinate:

$$\frac{\partial p}{\partial y} = 0 \Rightarrow p = p_e(x) \tag{2.6}$$

The next step is to perform the dimension analysis as has been done for the y-momentum equation, but this time for the streamwise direction or x:

$$\begin{array}{ccccccccc}
\frac{\partial u}{\partial t} & + & u\frac{\partial u}{\partial x} & + & \nu\frac{\partial u}{\partial y} & = & -\frac{1}{\rho}\frac{\partial P}{\partial x} & + & \nu\frac{\partial^2 u}{\partial x^2} & + & \nu\frac{\partial^2 u}{\partial y^2} \\
\frac{U_0^2}{L} & & \frac{U_0^2}{L} & & \frac{\delta U_0}{L}\frac{U_0}{\delta} & & \frac{1}{\rho_0}\frac{\rho_0 U_0^2}{L} & & \frac{\nu_0}{L^2}U_0 & & \frac{\nu_0}{\delta^2}U_0 \\
1 & & 1 & & 1 & & 1 & & \frac{1}{Re} & & \frac{1}{Re}\left(\frac{\delta}{L}\right)^2
\end{array}$$

Again, the third row is the result of multiplying the second one by $\frac{L}{U_0^2}$. It is possible to observe that the four first terms have an order of the unity while the fifth one would be negligible when the Reynolds number is considerably high, thing that happens. Therefore, the last term is the only one that takes into account viscosity and the only consistent solution to keep it is to say that the last term is approximately of order 1, which results in an estimation of the boundary-layer thickness:

$$\frac{\delta}{L} \sim \frac{1}{\sqrt{Re}} \tag{2.7}$$

The equation above implies that for really high Reynolds numbers, the boundary-layer thickness is very low compared to the characteristic length.

The consequence of the dimensional analysis is a significant simplification of the Navier-Stokes equations which models the behaviour of the flow in the region close to wall. Finally the 2D boundary-layer equations are:

$$\begin{cases}
\dfrac{\partial u}{\partial x} + \dfrac{\partial v}{\partial y} = 0 & (2.8) \\
\dfrac{\partial u}{\partial t} + u\dfrac{\partial u}{\partial x} + v\dfrac{\partial u}{\partial y} = -\dfrac{1}{\rho}\dfrac{\partial p_e}{\partial x} + \nu\dfrac{\partial^2 u}{\partial y^2} & (2.9)
\end{cases}$$

together with the initial and boundary conditions:

$$\begin{aligned} \text{IC}: \quad & u(x = x_0, y) = u_{in}(y) \\ \text{BC}: \quad & u(x, y = 0) = 0 \\ & v(x, y = 0) = 0 \\ & u(x, y \to \infty) = u_e(x) \end{aligned}$$

It is important to mention that u_e is the velocity at the wall obtained using the outer flow, which is controlled by the equation:

$$u_e \frac{du_e}{dx} = -\frac{1}{\rho} \frac{dp_e}{dx} \tag{2.10}$$

Therefore, a procedure used in some simulation codes to solve viscous flows is to firstly solve the Euler equations and after that use its results as boundary and initial conditions to solve the boundary layer equations. In addition, if the flow is considered steady $\left(\frac{\partial}{\partial t} = 0\right)$, equations 2.8 and 2.9 are parabolic so they can be solved using a marching scheme which is much easier than have to solve the whole system at once as for elliptic equations.

2.4 DESCRIPTIVE PARAMETERS OF THE BOUNDARY LAYER

In order to describe the boundary layer several parameters must be introduce. That is the goal of this section, give a definition of the most important parameters that describe the problem.

Maybe, the most relevant parameter is the boundary-layer thickness. A natural choice is to use the value of y at which the streamwise velocity u equals 99% of the free-stream velocity U_0 :

$$\delta_{99} = y : u(x, y) = 0.99 U_0 \tag{2.11}$$

Although it is a very intuitive definition, it is a poor conditioned quantity as requires to measure small velocity differences. For this reason, integral measurements have been developed as they result more reliable in some situations.

The concept of displacement thickness comes from the idea of mass flow conservation. It is known that for the viscous flows there exist a reduction in the flow rate that do not occur in the inviscid flows. By equalising that loss due to friction to the one that would occur in an inviscid flow the displacement thickness appears. It is better understand by looking at image 2 below, where the shadowed areas are the loss mentioned.

Mathematically, applying mass flow conservation and assuming incompressible flow, the displacement thickness is defined as:

$$\delta^*(x) = \int_0^\infty \left(1 - \frac{u(x,y)}{U_0}\right) dy \tag{2.12}$$

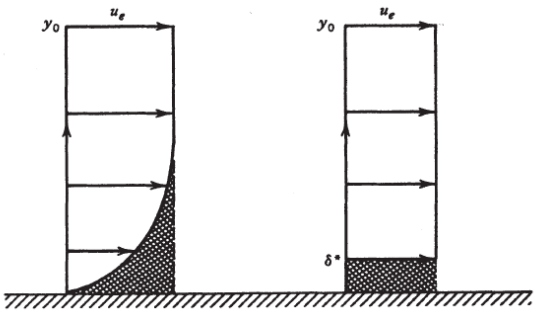

Figure 2: Displacement thickness graphical interpretation [2]

The momentum thickness follows a similar principle to the displacement thickness but takes into account the flux instead of flow rate, so it is defined as:

$$\theta(x) = \int_0^\infty \frac{u(x,y)}{U_0}\left(1 - \frac{u(x,y)}{U_0}\right) dy \tag{2.13}$$

Using the different scale lengths, several Reynolds numbers can be defined:

$$Re_x = \frac{U_0 x}{\nu}; \qquad Re_{\delta_{99}} = \frac{U_0 \delta_{99}}{\nu}; \qquad Re_{\delta^*} = \frac{U_0 \delta^*}{\nu}; \qquad Re_\theta = \frac{U_0 \theta}{\nu}; \tag{2.14}$$

Another very important parameter is the wall shear stress which represents the shear force per unit area at the wall and determines the friction drag. It is defined by:

$$\tau_w(x) = \mu \left(\frac{\partial u(x,y)}{\partial y}\right)_{y=0} \tag{2.15}$$

The normalization of wall shear stress is done using the dynamic pressure given as result the skin-friction coefficient:

$$c_f = \frac{\tau_w}{\frac{1}{2}\rho U_0} \tag{2.16}$$

There are other parameters that help to describe the boundary layer but they are much more specific to a single case of boundary-layer, so here the most general ones, those that can be used in any case are summarised.

2.5 BOUNDARY LAYER OVER A FLAT PLATE

One of the most studied cases and also one of the simpler ones is the one in which a boundary-layer is formed over a flat semi-infinite plate without a pressure gradient. It was Heinrich Blasius in 1908 the first to analyse this flow case applying the recently introduced boundary-layer equations. The set up it is shown in figure 3.

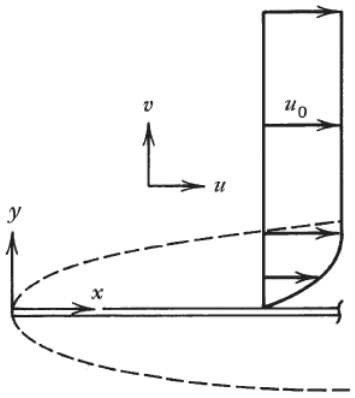

Figure 3: Blasius flow: flat plate in uniform stream [2]

Considering constant velocity at the outer flow, the boundary and initial condition are:

$$\begin{aligned} \text{IC}: \quad & u(x = x_0, y) = u_0 \\ \text{BC}: \quad & u(x, y = 0) = 0 \\ & v(x, y = 0) = 0 \\ & u(x, y \to \infty) = u_0 \end{aligned}$$

The boundary-layer equations are:

$$\begin{cases} \dfrac{\partial u}{\partial x} + \dfrac{\partial v}{\partial y} = 0 & (2.17) \\ u\dfrac{\partial u}{\partial x} + v\dfrac{\partial u}{\partial y} = \nu\dfrac{\partial^2 u}{\partial y^2} & (2.18) \end{cases}$$

As the equations show, the Blasius problem is a non-linear partial differential system that does not have a simple closed-form solution. Because of that, the successful approach is to use the similarity method. Then, is needed to find the proper quantities to convert the current variables into non-dimensional variables and by that try to

transform the PDE system into an ODE. The use of the stream function is helpful for that purpose. Here are summarized the variables involved in the process:

$$\eta = \frac{y}{\sqrt{\frac{\nu x}{U_0}}}; \qquad f(\eta) = \frac{\psi}{\sqrt{\nu x U_0}} \tag{2.19}$$

Applying the continuity equation and the stream function relations it is possible to find that:

$$u^* = f'(\eta); \qquad v^* = \frac{1}{2}\left(\eta f'' - f\right) \tag{2.20}$$

If those expressions are introduced into the momentum equation (eq 2.18) the final ODE is obtained together with new boundary conditions:

$$f''' + \frac{1}{2} f f'' = 0 \tag{2.21}$$

$$\begin{cases} f(0) = & f'(0) = & 0 \\ f'(\infty) = & 1 \end{cases}$$

The problem is solved using numerical methods suitable for non-linear equations and finally gives a value for the boundary-layer thickness using the $0.99U_0$ velocity:

$$\frac{\delta_{99}}{x} = 4.9\sqrt{\frac{\nu}{xU_0}} = 4.9 Re_x^{-1/2} \tag{2.22}$$

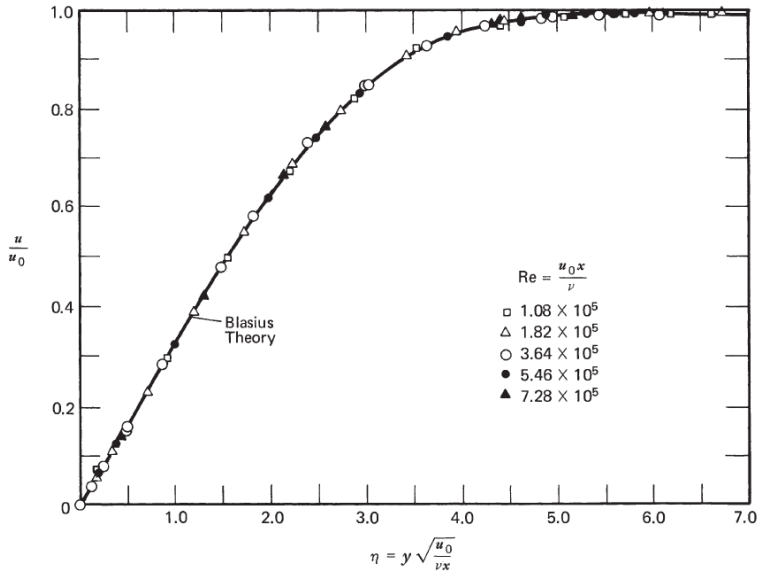

Figure 4: Results of experiments at five different x locations compared with analytical result [2]

Figure 4 shows the agreement between the experimental data and the analytical results exposed before. It also shows that the result does not depend on the Reynolds number when using the self-similar scale η.

Briefly explaining how the Blasius boundary layer has its purpose. The Blasius solution is actualy really important for the project as it has been used as an initial condition for some of the simulations together with suction. The transition from a simple Blasius profile to an ASBL is studied in later sections so it was important to give a perspective of the flow case.

The flow case of the laminar asymptotic suction boundary layer has the singularity of being one of the few analytical solutions to the Navier-Stokes equations. Its derivation is not included in this chapter because it will be studied more in depth in later chapters.

3 METHODOLOGY

The aim of this chapter is to provide an explanation of the method used to analyse the intended flow, the asymptotic suction boundary layer. In order to do that the key concepts of the CFD procedure employed are briefly explained as well as the software used to perform the simulations, SIMSON and MATLAB. Similar to what is done for experimental procedures, the set-up of the simulation is described and discussed. Finally, a validation of the code is done just to ensure that it is working as expected.

3.1 WHY CFD?

One century ago, when the aviation started its development, the only available methods to acquire new knowledge were through experiments (pure empirical) or using analytical procedures (pure theoretical) that later must be proven by the experiments. That approach was extremely slow and costly for engineering design which requires to change features constantly. It was not until the decade of the 60's when the Computational Fluid Dynamic became an useful tool in engineering analyses. The appearance of CFD coincided with the development of new and more powerful computers as the effectiveness of this kind of analysis is closely related to the processing power of computers. This is one of the reasons why CFD is so extended today in almost every field of engineering, as the computational power of a today's simple laptop is much greater than the corresponding to any supercomputer of the 60's.

The impact is so great that the CFD can be considered as "the third branch" of fluid mechanics [16]. However, the CFD has some limitations that are inherent to the physical models incorporated in the equations and in the boundary conditions as the results of the computations would be as valid as the models used. This problem is specifically relevant for turbulent flows where the models are quite complex and an statistical approach is needed. In addition, the accuracy of the calculations is influenced by the truncation error of the algorithm and the discretization employed as well as the round-off error of the machine.

In fact, the CFD has a considerable number of advantages. For aerodynamic purposes for example, performing several simulations using CFD is less expensive than doing experiments in a wind tunnel and the difference in price will continuously grow as the computers become more powerful. Using the example of the wind tunnel, in aviation or the car industries the conditions that must be recreated inside the tunnel are very extreme, due to the size of the real machines and the velocities that they reach.

As a consequence, there are many flow cases that are extremely difficult to recreate in a controlled experiment but are relatively easy to simulate with the proper software and the adequate computational power. To that must be added that the experiments deal with accuracy problems derived from measurement equipment and that measuring some flow parameters in an experiment become a challenge, while CFD provides all the flow features asked directly. The speed of the simulations is also a parameter to take into account as they can be much faster than performing experiments in the general case. The flexibility of CFD, the ability to change any feature of the simulations easily and quickly, has become the main advantage for the engineering design process as it allows to perform parametric studies quite fast. In fact, in the last few years a lot of CFD studies has been made in the aerospace field. Concretely, wing sections were studied in depth even using the most advanced techniques and DNS, some examples are [17], [18] and [19].

CFD is a tool that properly used can help to unravel the problems of turbulence by being able to deal with the Navier–Stokes equations at sufficient small scales that the initiation of turbulence can be captured and studied. Within this field of action is where this project belongs. Then, the selection of CFD as the tool to analyse the ASBL is justified by all the advantages mentioned in the last paragraph.

3.2 DIRECT NUMERICAL SIMULATIONS

As in every science field, the final goal is to find a relatively simple and tractable model or theory of the phenomenon studied. In the case of turbulent flows, that goal has become a real challenge due to the complexity of turbulence. The fact that the velocity field of turbulent flows is three-dimensional, time-dependant and random and also that the biggest length scales are within the range of the characteristic lengths raise the difficulty so much that there are no prospects of an analytic theory or model of turbulence. Then the common method to study that kind of flows is CFD and rely on the increasing computational power of computers. However, within the CFD methodology there are several computational approaches to study turbulence: direct numerical simulations (DNS), large-eddy simulations (LES) and Reynolds-averaged Navier–Stokes equations (RANS). Depending on the objective of the study to be perform an approach is more suitable than the others. The level of description, the cost and the accuracy are some of the parameters that intervene when deciding which approach is the best.

The DNS consists in solving the Navier-Stokes equations without using any model for turbulence. That means all the length and temporal scales must be resolved using the boundary and initial conditions appropriate to the flow considered. As a consequence of the need of capturing all the length scales, even the smaller ones, the Kolmogorov or the dissipation scale, the mesh must be adequate to this purpose which

implies a huge computational cost that restrict the use of DNS to small Reynolds numbers. However, among all the approaches is the easiest to understand conceptually and has the best accuracy and level of description. On the other hand, the RANS approach models the turbulence so the results highly depend on the model selected and so the accuracy and reliability of the data is not as good as in DNS but the computational cost is much lower. The LES approach is situated as mixture of both previous approaches because model only the length scales indicated, usually the smaller ones, saving computational cost compared with DNS.

The singularities of the DNS approach convert it in the most suitable method to study the turbulent behaviour of a wide range of flows. It allows to extract a considerable number of variables of interest, not only from the mean flow but also from the perturbations, giving a clear picture of the turbulent structures formed within the flow from the smaller to the bigger ones. It is a method that is able to supplement the data from experiments avoiding possible disturbance of the measurement apparatus. However, due to its limitations concerning the computational cost, it is not the most suitable approach to design a wing or an aileron but it helps to understand how the turbulence is generated there and so how to create the models used in RANS simulations.

For these reasons, in order to carry out the simulations of this project the approach followed was DNS, as the key goal is to understand what is happening in the boundary-layer when suction is applied. In addition to DNS, some LES simulations have been done although only a very few scales were not solved so they were close to be a full DNS.

3.3 SOFTWARE

Once the type of methodology that it is going to be implemented has been presented and justified, it is possible to continue with the tools needed to carry out the project. In this case, which software has performed the simulations and how the data was treated and post-processed later.

3.3.1 SIMSON

SIMSON is a software package developed by KTH which solves the Navier–Stokes equations for incompressible channel and boundary-layer flows, an example of it is the paper by Bobke et al. [20] on pressure-gradient turbulent boundary layers on flat plates. It is possible to run the code as a solver for DNS, resolving all the time and length scales, but it can also be run as a LES, where it is possible to choose the most suitable model for solving smaller scales. The streamwise and spanwise directions are discretized using Fourier series while the normal direction is discretized using Chebyshev series. For the temporal discretization, a third order Runge–Kutta method

was used for the advective and forcing terms while for the viscous terms a Crank–Nicholson method was employed. Both temporal and spatial simulations can be done using SIMSON which gives flexibility for choosing the boundary and initial conditions. The code can be run both in serial or in parallel as it is possible to choose the number of threads to work with.

The solver is implemented with Fortran 77/90 which is needed for compiling. It must be run in an Unix like platform, in this case Linux was employed. For this purpose, it was needed to learn how the Unix environment worked. For further information on the details of the numerical method used in SIMSON it is recommendable to look at the SIMSON manual [21].

The following table summarizes the most important files employed to run the simulations. They include a brief description of its purpose and they are sorted by its actual order of correct execution:

1. **par.f** → Sets the number of spectral modes of the simulation and the number of threads, as well as other critical parameters.
2. **fsc.i** → Introduces the key parameters to create a similarity solution.
3. **fsc** → Executable that computes the similarity solution from the data of fsc.i
4. **bls.i** → Sets the box size, the Reynolds number, the flow type and the disturbance of the initial conditions.
5. **bls** → Executable that generates the initial flow field from the data of bls.i
6. **bla.i** → Sets the time of simulation, activates the suction and sets the output files.
7. **bla** → Main program, computes the final solution.
8. **rit** → Executable that plots information from instantaneous velocity fields.
9. **pxyst** → Executable that plots xy-statistic

As a final comment is important to mention that every executable file must be compiled within its own directory and using the correct par.f file.

3.3.2 MATLAB

MATLAB is a numerical computing environment very useful for engineering and applied mathematical purposes.It allows to plot and handle data in a very simple way thanks to its high-level language. Due to that, MATLAB was used within this project in order to post-process the data obtained with SIMSON. By doing this, more intuitive plots were done. Matlab was also used to scale the necessary data, for example convert from free-stream scaling to inner scaling using plus units.

3.4 SIMULATIONS SET-UP

The aim of this section is to provide a view of the general set-up of the several simulations performed. As a variety of simulations have been made: using different resolutions and box sizes, temporal and spatial and also laminar and turbulent cases; it is only discussed the most general aspects of the set-up. Further details will be explained in the following chapters together with the results.

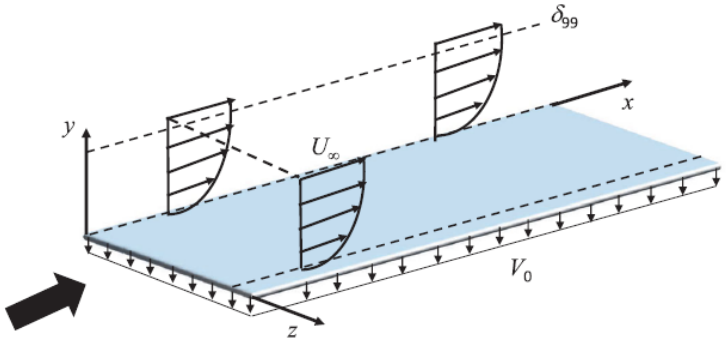

Figure 5: Sketch of a temporally developing asymptotic suction boundary layer over a flat plate with its coordinate system and notation [3]

In figure 5 the basic set-up of the simulations is represented together with the coordinate systems XYZ. The first step is to determine the dimensions of the computational box or the domain size. The influence of it in the laminar studies is negligible as long as the vertical coordinate is big enough to contain the boundary layer, but in the case of turbulent flows the computational box has a very significant role as it must be sufficiently big to comprehend the vortexes and turbulent structures. The domain size is represented as $L_x \times L_y \times L_z$. Similarly, the number of spectral modes in each direction is represented as $N_x \times N_y \times N_z$. It can be understood as number of points in each direction or in other words, determines how coarse or fine the mesh could be, also named as resolution. It has a direct impact in the accuracy of DNS as it must be sufficiently small to notice the tiniest structures of turbulence. In the horizontal plane, the resolution is constant while in the vertical direction the mesh is very fine close to the wall while coarser at he free-stream, effect of using Chebishev polynomials.

In order to perform the laminar simulations, the spectral modes of the z direction, N_z, were set to 1. This is analogous to transform the 3D domain into a 2D, which avoids the turbulence to appear as the turbulence is a three-dimensional phenomenon.

It is also important to know that everything was re-scaled using the initial displacement thickness, δ_0^*. The reason behind this decision will be explained in the next chapter. Using this scaling leads to use the following Reynolds number:

$$Re = \frac{U_0 \delta_0^*}{\nu} = 333 \tag{3.1}$$

This Reynolds number is characterized on the asymptotic state of the boundary layer with suction, which, as it will be showed in the next chapter, indicates the rate of suction of the simulation. Then, setting that Reynolds number is equivalent to set the suction rate to 0.003, which is a proper value in order to avoid relaminarisation and to sustain turbulence [3]. It is important not to confuse that Reynolds number with the initial Reynolds number of the simulation, which is an indication of how viscous the fluid is in relation with velocity. For almost all the simulations in the thesis, it is set to 450.

For all the flows simulated with SIMSON, the boundary conditions in the horizontal directions, x and z, are periodic as a requirement of the spectral method used to discretize the domain. By doing this, the computational cost is reduced considerably although it basically consists in assuming that what exits by the outlet enters again by the inlet. However, in the vertical direction it is different as the boundary conditions differ depending on the flow type used. In order to simulate the ASBL the strategy followed was to implement a constant suction by subtracting the suction velocity V_0 to the Navier–Stokes equations in the vorticity form. On the contrary, the free-stream boundary conditions are set differently. For the case of ASBL they are set almost for every simulation as Dirichlet Boundary conditions:

$$u|_{y_L} = U \qquad v|_{y_L} = V \qquad w|_{y_L} = W \tag{3.2}$$

The value y_L represents the farthest distance from the wall, which in theory should be infinite but the discretization method can only handle finite domains. This can lead to errors so, for the spatial simulations an improvement was made in the boundary conditions by using Neumann conditions:

$$Du|_{y_L} = DU \qquad Dv|_{y_L} = DV \qquad Dw|_{y_L} = DW \tag{3.3}$$

Everything said about the boundary conditions is completely true for the temporal simulations. Nevertheless, for the spatial ones, there exist some important features to add. In spatial simulations, the streamwise direction cannot be idealized as periodic. However, the periodic boundary conditions are required by the Fourier discretization so what it is done is to add a fringe region downstream of the domain, where the disturbances are damped and the flow is returned to the desired inflow condition. In addition, for the spatial simulations a trip force is added in order to generate turbulence.

For the laminar simulations the initial condition is a Blasius velocity field that simulates the state of the flow before adding any suction. For the turbulent temporal case, the initial condition is the laminar ASBL velocity field. It is important to say that the initial velocity field includes an small perturbation that grows with time in order to generate turbulence. For the spatial case, this is reinforced by the tripping.

Finally, in order to perform the LES simulations, the ADM-RT (Approximate Deconvolution Model–Relaxation Term) model was used, which acts directly on the velocity components with a force. By doing this, only the smallest scales are affect by the high-order filter H_N. The forcing is represented as:

$$\frac{\partial \tau_{ij}}{\partial x_j} = \chi H_N * \bar{u}_i \tag{3.4}$$

3.5 DNS VALIDATION

In every CFD project there must be a validation part where it is checked that the code employed is working the way expected. For this project, although SIMSON has been used for several papers and researches so it is been proved that it works, it was decided to run a case as validation. In fact, more than a validation of the code, was closer to a certification that the author knows how to handle SIMSON.

The validation was carried out using one of the most classical examples of DNS: the channel flow by Kim et al. [22]. The set-up was practically identically to the one in Kim but as there was impossible to find the data set of that simulation, a newer example was taken: the study by Lee et al. [4] in 2015 whose data set are available at [23]. The conditions are in very good agreement with Kim.

Case	Re_b	Re_τ	L_x	L_z	Δx^+	Δz^+
Lee	2857	182	8π	3π	4.5	3.1
Kim	2800	180	4π	2π	12	7
Simson	2800	180	2π	π	17.6	8.83

Table 3.1: Performed simulations to do the validation of Simson

Table 3.1 summarizes all the information of the cases compared. Re_b is the Reynolds number based on the bulk velocity and half the height of the channel. In order to run the simulation in SIMSON, this Reynolds was converted to Re_{cl} which is based on the centreline velocity and is the one used by SIMSON, $Re_{cl} = 4200$. The other Reynolds number appearing is the friction one, Re_τ which will be defined in the following

chapters. For the channel flow, it is needed to establish it as a measure of flow forcing. The domain in the stream and spanwise directions is normalised by half the height of the channel. Finally, Δx^+ and Δz^+ make reference to the grid spacing in the horizontal plane in plus units. It can be seen that the spacing used in the Lee and Moser paper is much fine than the one used for Kim and the case ran with SIMSON. The purpose of that is, mainly the saving of computational effort, but also prove that a DNS can be done with a coarser grid.

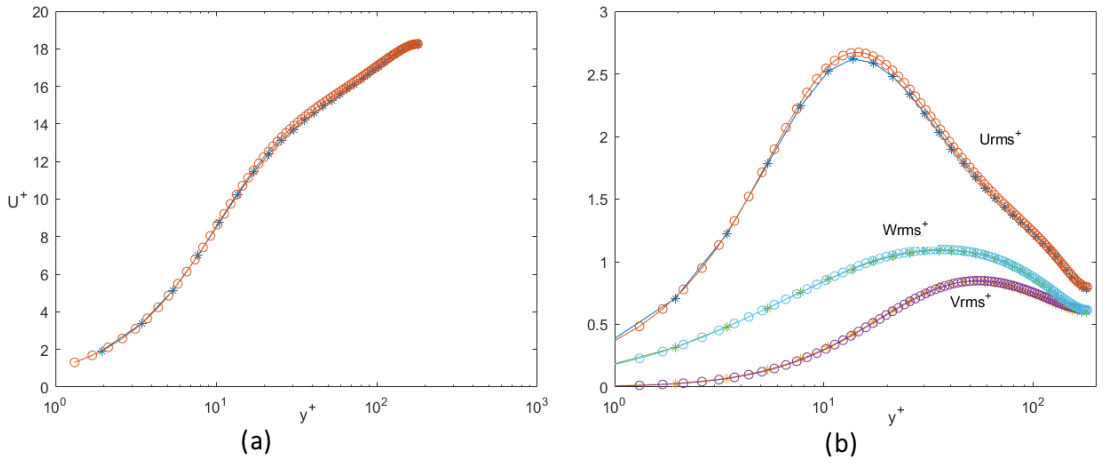

Figure 6: (a) Velocity profiles in wall units. (b) Components of Reynolds stress tensor. For both, line-circle corresponds to Lee et al. [4] while line-star corresponds to SIMSON.

The figure above shows a very good agreement between the data from Lee ET AL. [4] and the simulation performed with SIMSON, at both, the velocity profile and the Reynolds stresses. From this, is possible to ensure that SIMSON is working as expected and also that the grid is not needed to be so fine as in that paper. However, using a DNS with SIMSON is not always possible due to computational limitations. There are some cases within the project that, due to its massive length in space, the DNS is discarded in favour of a LES in which only the smallest scales are modelled.

4 LAMINAR ASBL

This chapter deals with the laminar state of the ASBL and it is subdivided into two different sections. The theory part consists on showing the analytical form of the characteristic variables of the boundary layer with suction from the laminar point of view: velocity profile, displacement thickness, etc. Meanwhile, in the second part the results from the laminar simulations are exposed and explained. Although the laminar state could not be of a great practical importance, it is crucial in order to properly understand the next chapter which deals with turbulent state of ASBL.

4.1 THEORY

In order to characterise the asymptotic state of the laminar boundary layer with suction, the first step is to obtain the velocity profile of it, then so knowing how the speed varies depending of the coordinates. To do so, the general equations of the incompressible boundary layer (eq. 2.8 and 2.9) are used but modifying the boundary conditions. They are redefined as follows:

$$\begin{aligned} \text{IC}: \quad & u(x = x_0, y) = u_{in}(y) \\ \text{BC}: \quad & u(x, y = 0) = 0 \\ & v(x, y = 0) = -V_0 \\ & u(x, y \to \infty) = u_e(x) \end{aligned}$$

In addition to the change in the boundary conditions, some more assumptions need to be made. As it is considered that the boundary layer is going to reach an asymptotic state, which means that it is supposed to stand-still, then it can assumed that the boundary layer is steady, no changes in time $\frac{\partial}{\partial t} = 0$, and also that it is fully-developed in the x direction, it does not experiment variation in that direction $\frac{\partial}{\partial x} = 0$. If the section about the Blasius boundary layer is remembered, this last assumption could not be made, as the boundary layer grew constantly with x, which is a severe complication saved for this case by assuming the asymptotic state. It is also assumed that there is no pressure gradient. Firstly, those new conditions are applied to the continuity equation (eq 2.8) which leads to the following expression:

$$\frac{\partial v}{\partial y} = 0 \tag{4.1}$$

It can be translated by saying that the vertical velocity is not changing along the y direction. If that is joined to the knowledge of the vertical velocity at the wall, established by the boundary conditions, it can be implied that the vertical velocity v in the boundary-layer is constant and equal to the suction speed, $v = V_0$. By doing the same analysis to the momentum equation (eq 2.9), the following differential equation is reached:

$$-V_0 \frac{\partial u}{\partial y} = \nu \frac{\partial^2 u}{\partial y^2} \tag{4.2}$$

After integrating equation 4.2 once, a linear differential equation is obtained which is subjected the consequent linear analysis, leading to a final expression of the horizontal velocity in function of the y coordinate, $u(y)$:

$$u(y) = U_0 \left(1 - e^{-\frac{V_0}{\nu} y}\right) \tag{4.3}$$

Once the velocity profile is obtained, it is possible to calculate other parameters that help to characterize the boundary layer, which were those introduced in chapter 2. It is convenient to start defining the displacement thickness using the formula from equation 2.12:

$$\delta^* = \int_0^\infty \left(1 - \frac{u(y)}{U_0}\right) dy = \frac{\nu}{V_0} \tag{4.4}$$

The expression of displacement thickness implies that the boundary-layer thickness in its asymptotic state depends basically on the suction speed and the fluid's type. The reason of adimentionalising the whole problem using the displacement thickness is comprehended when a new y coordinate is defined using it and applied to the velocity profile:

$$y^* = \frac{y}{\delta^*} = \frac{V_0}{\nu} y \quad \rightarrow \quad u(y^*) = U_0 \left(1 - e^{y^*}\right) \tag{4.5}$$

The expression 4.5 justifies the decision of using δ^* as adimentionalisation factor, as it reduces the velocity profile to a simple exponential function. Following the reasoning, the Reynolds number can be also be defined using the displacement thickness:

$$Re_{\delta^*} = \frac{U_0 \delta^*}{\nu} = \frac{U_0}{V_0} = \frac{1}{\Gamma} \tag{4.6}$$

This Reynolds number has the advantage of characterizing the ASBL as it relates the velocity of the free-stream with the suction velocity, whose ratio is called Γ or suction rate. The correct assigned value of Γ, and so then of the Reynolds number, determines the existence or not of a turbulent state as too much suction can lead to relaminarisation of the boundary layer. Many studies deal with the determination of a critical suction rate but there was a final agreement that established the critical

Reynolds number near 270, that it is why the Reynolds number of the asymptotic state, which is the same as establishing the suction speed, was chosen to be 333 which can be considered a save value to ensure turbulence [3].

It is also important to mention the friction-related parameters previously defined in chapter 2:

$$\tau_w(x) = \mu \left(\frac{\partial u(x,y)}{\partial y} \right)_{y=0} = \rho U_0 V_0 \tag{4.7}$$

$$c_f = \frac{\tau_w}{\frac{1}{2}\rho U_0} = 2\frac{V_0}{U_0} = \frac{2}{Re_{\delta^*}} = 2\left(\frac{u_\tau}{U_0}\right)^2 \tag{4.8}$$

Both parameters above are independent from the regime of the flow, which means that it is valid for both laminar and turbulent regime. It is also possible to see that a certain balance exists between the friction and the suction, as with higher suction higher shear flow on the wall. That increasing in friction answers to the rise of momentum due to the suction.

4.2 SIMULATIONS

After introducing the main aspects of the ASBL in a theoretical way, it is possible to perform the simulations and analyse the results expecting a determined behaviour of the flow. In this section the behaviour of the boundary layer under suction is investigated from both the temporal and the spatial point of view individually, studying its evolution from a simple Blasius profile to the characteristic asymptotic state, expected outcome of suction. Finally, both evolutions, spatially and temporally are compared.

4.2.1 Temporal simulations

In this section, the results of the temporal simulation are presented. The objective is to observe and understand how the boundary layer evolves from a Blasius profile to the asymptotic state and to quantify the convergence into such state. It is important to remember that, in a laminar temporal simulation, the boundary conditions on the horizontal plane are periodic, which makes less important the dimensions in that plane than the vertical dimension. As mentioned previously, a laminar approach requires the use of only 1 point in the spanwise direction converting that direction in inconsequential. The parameters of the simulation are summarized in table 4.1:

The initial condition of the simulation was, initially, a Blasius profile with a displacement thickness equal to the unity. The goal of this was to simplify the scaling of the whole simulation. The initial condition tries to replicate the conditions that would appear on wind-tunnel, where is nearly impossible to apply suction during all along

Name	Re_{δ^*}	L_x	L_y	L_z	Resolution	Time
lam450t	450	100	50	100	$4 \times 65 \times 1$	3000

Table 4.1: Set-up data for the temporal laminar simulation of ASBL. The Reynolds number, the box dimensions and the time, which is in convective time units, are scaled using the displacement thickness, δ^*.

of it and so, on the initial part of it a simple Blasius boundary layer is developed. However, in the temporal simulation in which the initial thickness is equal to one, that early state of a possible wind-tunnel experiment is not effectively replicated, as in a wind-tunnel that boundary layer continuously grows while the suction is not applied. After the first results, the initial displacement thickness was changes in order to match the boundary-layer thickness of the spatial simulation just before suction. The results showed in this section correspond to this new initial condition.

Before starting with the results, it is important to mention a detail quite relevant in laminar simulations. In contrast with turbulent simulations where there exist a lot of variability, the laminar cases are, in some ways "straight forward", so they tolerate worse any possible disturbance and consequently they are more susceptible to be perturbed. Keeping this in mind, the simulations carried out with SIMSON employs an adaptive method to determine the time step, Δt, which is based on the CFL condition. It is a necessary condition for convergence as it ensures the stability of the method by relating the necessary time step with the convective speed and the grid resolution limiting the speed at which information travels through the grid. This relation is mathematically described by the CFL number or Courant number which should be less than a certain value, 1 for explicit methods:

$$C = \frac{u\Delta t}{\Delta x} \leqslant 1 \qquad \textbf{Unidimensional Courant number} \tag{4.9}$$

Then, the time step is limited by the resolution of the simulation so the finer the grid, the smaller the time steps are required to satisfy the condition before observing numerical stability problems. In order to use the resolution that appears in table 4.1, the CFL parameter must be reduced in order to avoid to reach the adequate values of time step that avoids the instability, which is more exigent in the laminar cases. For this reason the CFL number used in the temporal laminar simulations is 0.2 instead of using 0.8 which is the standard value for all the simulations in SIMSON.

Once the simulation has been performed,the next step is to look at the velocity profile, for example, how the velocity changes with the vertical coordinate. The shape of that profile allows to know which is the state of the flow, so from it, it is possible to recognise if the boundary layer has reached the asymptotic state. As the simulation is

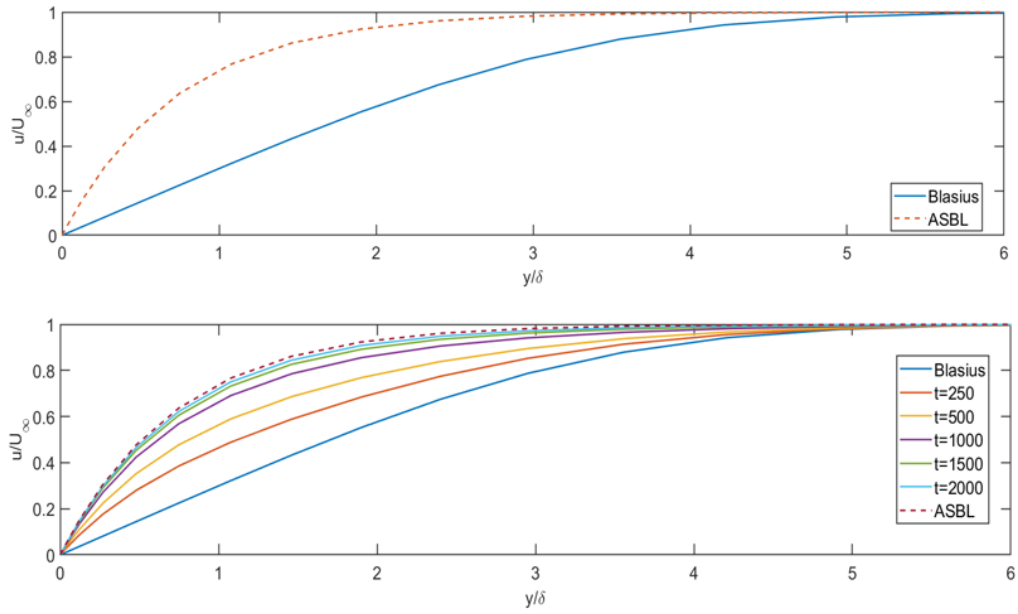

Figure 7: (a) Initial Blasius profile and the ASBL profile. (b) Several velocity profiles for different instants of time until the collapse to the ASBL. $Re = 450$ for both.

temporal, the idea is to compare those velocity profiles for different moments in time to know when the ASBL is achieved.

That temporal evolution is shown in figure 7. The first plot just shows the initial Blasius profile together with the analytic velocity profile corresponding to the laminar ASBL for the same Reynolds. As it can be seen, the difference between those two profiles is not very significant, which can mean that the convergence to the asymptotic state could be quick. The second panel shows the velocity profile at different instants of time allowing to discern the evolution of the boundary layer towards the asymptotic state. Due to the fact of the quick transition, at 1500 the profile is almost overlapped with analytic ASBL. This supports what was mentioned before, that the convergence is quite quick, which may be possible due to the proximity of the initial Blasius profile.

However, looking at the velocity profiles is not sufficient to asses if the the boundary-layer has converged to the ASBL. In order to make a correct scientific assessment of the convergence it is necessary a new parameter that evaluates the proximity of the whole velocity profile to the analytical ASBL. In the paper by Vinuesa et al. [24], the convergence of numerical simulations is studied and a convergence indicator is defined as the RMS (root mean square) norm of the deviation between the converged

state and the instant variable of interest. In this case, the analytic ASBL profile is compared to the different velocities profiles in time.

$$\epsilon = \left[\frac{1}{h}\int_0^h (\cdot)^2 dy\right]^{\frac{1}{2}} \tag{4.10}$$

Using ϵ as a convergence indicator for time evolution is possible to know if the simulation has reached the ASBL and how fast.

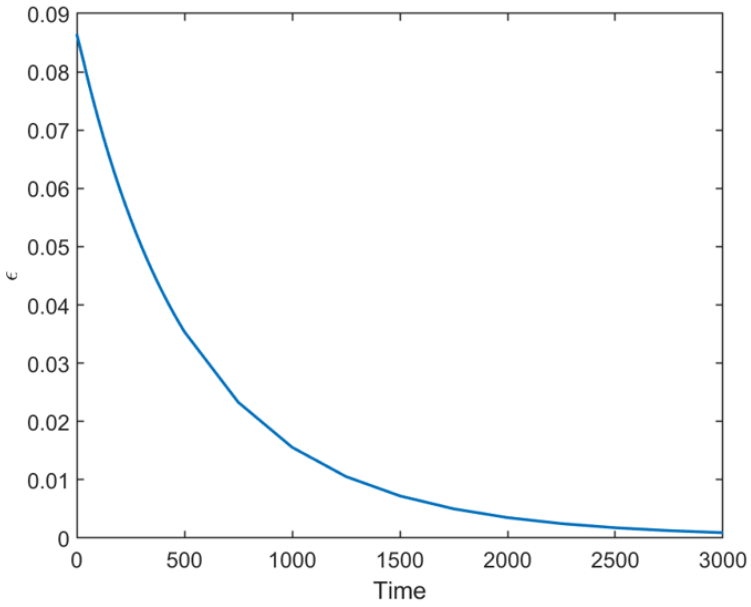

Figure 8: Convergence rate ϵ evolution with time

As expected, the behaviour of ϵ is of an exponential function that tends to zero in the infinity. The figure 8 shows exactly that result, a very steep slope towards zero in the first instants very characteristic of an exponential convergence. Again in the paper by Vinuesa et al. [24], a reference to know if the parameter investigated has converged is given. They say that when ϵ reaches an order of 10^{-3} it can be assumed that the simulation has reach the converged state. For the case studied here, ϵ reaches that approximate value around 1500 convective time units which can be corroborated the previous figure where the velocity profiles are almost overlapped.

A different option to check the convergence is to look at the characteristic properties of the boundary layer, like the shear force or the skin-friction coefficient. From the analytical result showed before it can be obtained the value of the skin-friction coefficient of the ASBL using the equation 4.8 in which the Reynolds number is involved. At the same time, the skin-friction coefficient can be also obtained by calculation the shear force deriving the velocity profile and so get a value of u_{tau} for each time. That

would be the approach form the simulation point of view while using the Reynolds can be an analytic approach. The advantage of this indicator is that is valid also for the turbulent regime.

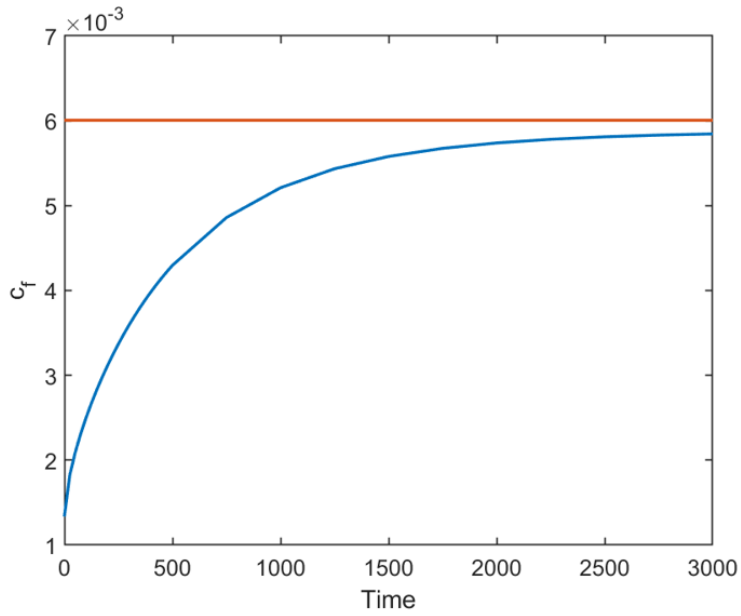

Figure 9: Skin-friction coefficient evolution with time. Red line represent the analytic value for the ASBL

It can be observed in figure 9 that the skin-friction coefficient quickly approaches the asymptotic value, at more or less 1500 time units. However, it does not stabilize until some time later when the c_f reach an stable state where it is parallel in the graph to the analytic value. The difference between them is of the order 10^{-3}, so it is almost negligible and can be said that the simulations has reached the asymptotic state, same conclusion as using ϵ.

4.2.2 Spatial simulation

As was mentioned before, temporal simulations does not provide a very realistic approach because they use periodic boundary conditions. In order to have a more realistic approach, a spatial simulation is implemented where the flow is allowed to freely develop in the streamwise direction, without the periodic boundary conditions. This kind of simulations help to understand how the boundary layer evolves in the x direction, not only in time. Although they provide a vision much closer to reality than temporal simulations, they are also much more computationally expensive as the domain size in the streamwise direction has an important impact, usually promoting to

use really long computational boxes. This fact is reflected on table 4.2 which is practically equal to table 4.1, except for L_x which is much bigger now and consequently, in order to maintain an acceptable resolution, the number of points in x has been increased. Again, as a laminar simulation, the spanwise direction has been neglected, fact that reduces the cost of the simulation. A sufficient amount of time needs to be specified in order to let the boundary-layer develop correctly, so 3000 convective time units were considered as a proper value as for this time in the temporal simulation the boundary- layer was already converged to asymptotic state.

Name	Re_{δ^*}	L_x	L_y	L_z	Resolution	Time
lam450s	450	3000	50	100	$1024 \times 65 \times 1$	3000

Table 4.2: Set-up data for the spatial laminar simulation of ASBL. The Reynolds number, the box dimensions and the time, which is in convective time units, are scaled using the displacement thickness, δ^*.

Regarding the initial conditions, for this simulation it is more complicated than for the temporal case. In order to replicate a more realistic situation, for time and x-coordinate zero the Blasius profile is the same as for the firstly done temporal simulation with displacement thickness of unity, howbeit it has been led the Blasius boundary-layer to develop until $x = 500$, point in which the suction is started to be applied. This kind of set-up is in better agreement with a possible experiment carried out in a wind tunnel. Nevertheless, it also brings some problems in order to compare it with the temporal case, as the suction is not applied to the same conditions of the Blasius profile.

In figure 10 it is possible to appreciate two boundary-layers spatially developed. In picture (a), it is represented the evolution of a simple Blasius boundary layer up until 500 space units. It is possible to see how it is continuously growing with the x-coordinate but it is also doing it in a decaying way, decelerating its growing. That first picture represent the initial conditions of the suction, as after $x = 500$ is applied. The second picture represents that change in the behaviour, from a continuously growing Blasius profile to the ASBL, asymptotically approaching the analytic profile. It is possible to observe that the suction rapidly affects the boundary layer as it considerably changes from $x = 500$, where the suction starts, to $x = 750$. By a distance of $x = 1500$, the simulation profile has already collapse with the analytic result meaning that it has reached the asymptotic state.

A very intuitive way to understand what is happening in the x-coordinate is to plot the boundary-layer thickness against that coordinate, so it is possible to see how quick the suction is affecting the boundary-layer. Figure 11 does exactly that:

Looking at the graphs it is easy to realise that the data only reaches $x = 2500$ although the domain is 3000 units. The reason of that is the fringe region that had to

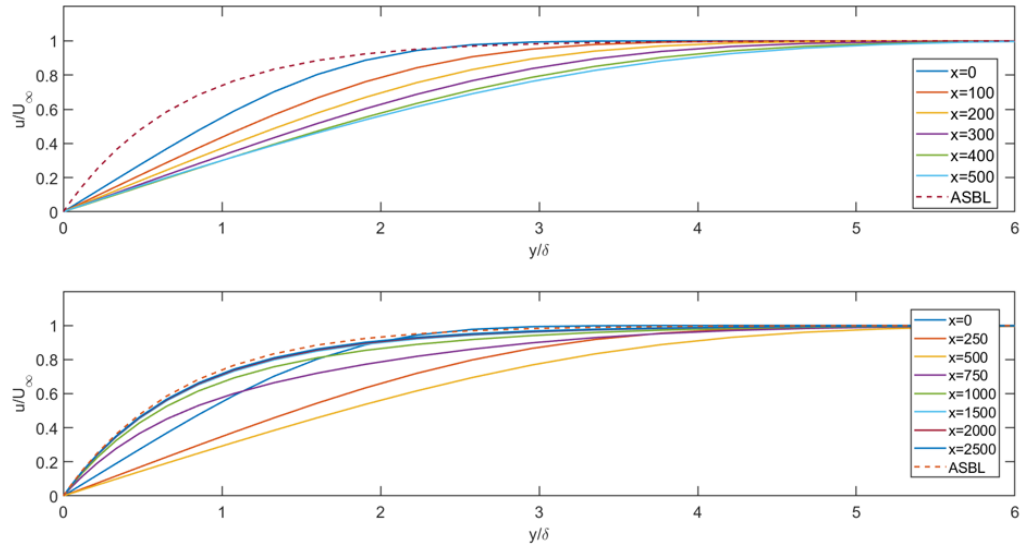

Figure 10: (a) Evolution of Blasius boundary layer until $x = 500$. (b) Spatial evolution of boundary layer applying suction after $x = 500$. $Re = 450$ for both.

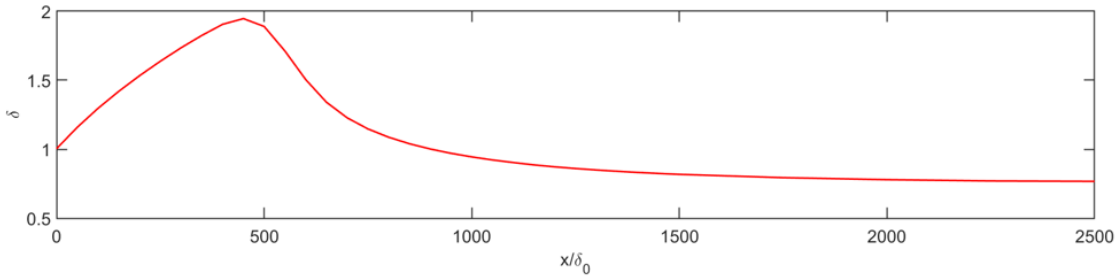

Figure 11: Displacement thickness evolution with the streamwise coordinate

be added in the simulation to be able to get rid of the periodic boundary conditions while using a spectral analysis. It is a kind of forcing that disturbs the flow around of it, so the results obtained in that zone would not have meaning.

As for the temporal simulation, the convergence needs to be evaluated in the proper way. In order to do this, the same parameters used before are valid now, ϵ and c_f. Both are represented in the figure 12. As it was expected, during the first 500 units the convergence is really bad, as the Blasius boundary layer is being developed. However, once passed this point the convergence starts to improve. In picture (a), ϵ decays very fast towards zero while in picture (b) the skin-friction coefficient approaches the expected value of the ASBL, 0.006. It is expected that, if the length of the domain is increased, the convergence would also improve although ϵ has already reached the

threshold of convergence, around the order of 10^{-3}, and so the decrease would be considerably slow.

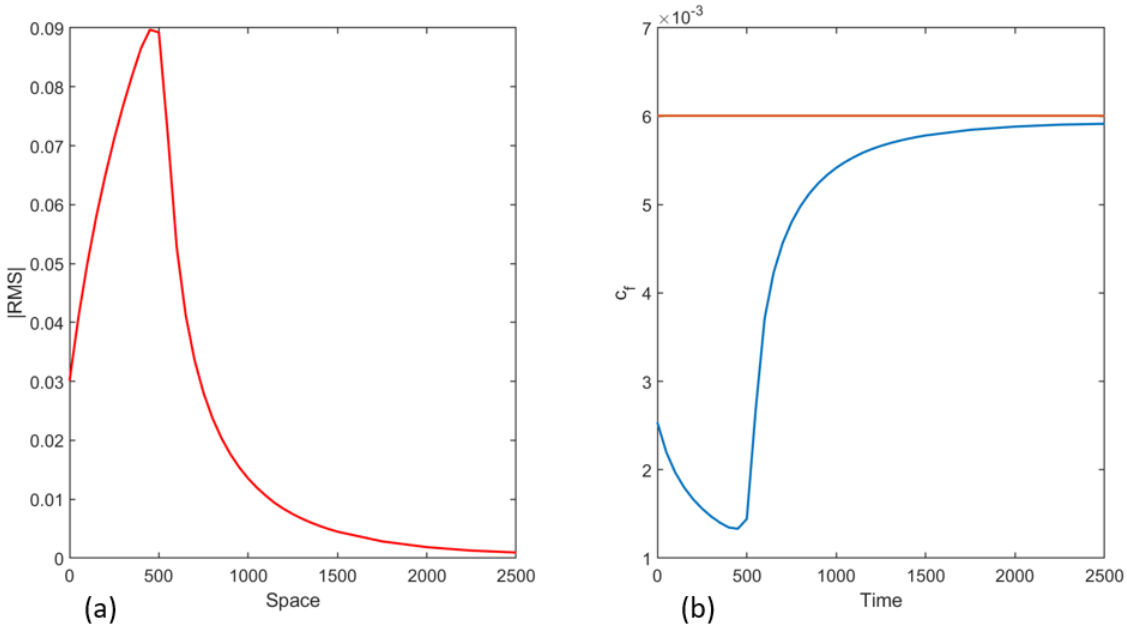

Figure 12: (a) Convergence of spatial simulation towards the ASBL measured with ϵ. (b) Convergence using the skin-friction coefficient.

In the next section, the differences between temporal and spatial simulations will be studied

4.2.3 Comparison

Once the temporal and the spatial simulations have been studied individually, it is convenient to compare both of them. Before starting with the comparison, it is important to comment that several modifications were needed in order to be able to compare the boundary layer evolution in space and time. The code SIMSON uses by default an initial displacement thickness, also used for scaling, of 1 unit, so the temporal simulation started with that value of initial thickness and then suction is applied. The problem was that, in the spatial simulation, the suction is applied after 500 space units and consequently the boundary layer got bigger, its thickness was almost doubled. Then, with these conditions, was not really correct to compare both simulations. In order to fix that, the code was modified to use as initial displacement thickness in the temporal simulation the corresponding thickness of the boundary layer in the spatial simulation just before suction was applied, $\delta^* \approx 1.9$. Another comment about the comparison is that the x coordinate was modified by relocating $x = 0$ at the point where suction be-

gin, the same of subtract 500 units to the whole coordinate. By doing this, the graphs are much easier to read and understand.

In order to compare the simulations, two parameters were selected because both of them are able to show how the boundary layer is approaching the asymptotic state. Those parameters are the convergence rate, ϵ, and the displacement thickness,δ^*. Also δ_{99} was obtained but it was not a really interesting parameter as the simulations are laminar so then the evolution was not properly shown, although for turbulent simulations it is really useful. The two parameters mentioned above are represented in the figure 13. Both figures show a similar trend, the boundary layer seems to develop faster in space than in time, at least in the laminar case. In addition, although figure (a) represents the convergence rate and figure (b) the displacement thickness, the curves are also very similar.

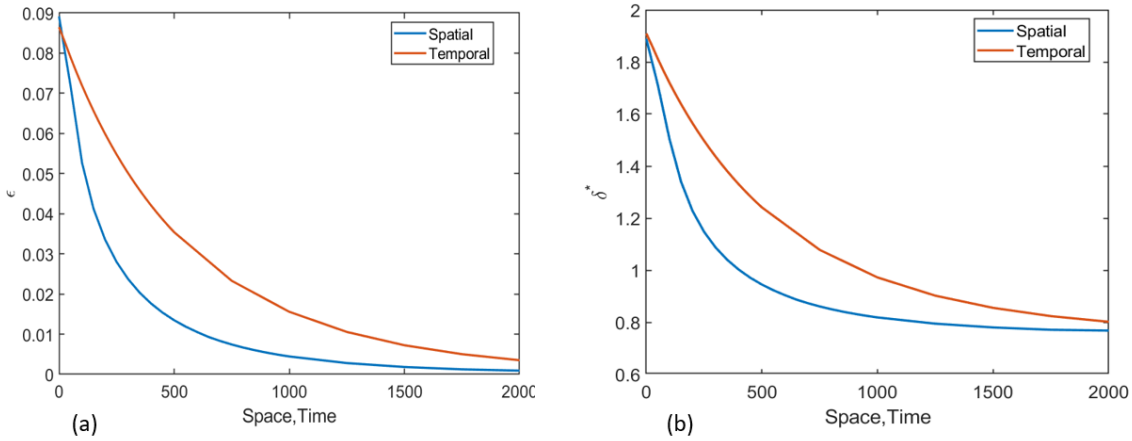

Figure 13: (a) Convergence rate, ϵ, in space and time. (b) Displacement thickness evolution in space and time.

However, stating that the boundary layer seems to develop faster in space than in time is not sufficient for researching purposes. It is necessary to find a quantitative relation between space and time that allows to estimate how much streamwise distance would be required to completely develop the ASBL for the corresponding required time to develop the boundary layer in a temporal simulation. By finding that parameter, the computational power required to make an spatial simulation, which is much more demanding, can be saved and just perform a cheaper temporal simulation.

The method employed to relate time and space was to connect them using the displacement thickness by the MATLAB function “interp1". This function interpolates a 1D vector data that, in this case is displacement thickness of the spatial simulation, at specific query points, which are the points of the displacement thickness of the temporal simulation, using a linear interpolation. Thanks to this function it is possible to obtain a vector of streamwise coordinate corresponding to the temporal points. The

blue line in figure 14 shows exactly that relation between space and time, result of the explained procedure. It can be seen that instead of having a linear behaviour it closer to a quadratic function. Nevertheless, as it is wanted to find the simplest relation as possible, a linear fitting was applied to that, resulting on the orange line. By doing so, the slope of the line correspond to the relation between space and time, which has the units of velocity. The correlation is:

$$u_T = \frac{x}{t} \approx 0.65 \tag{4.11}$$

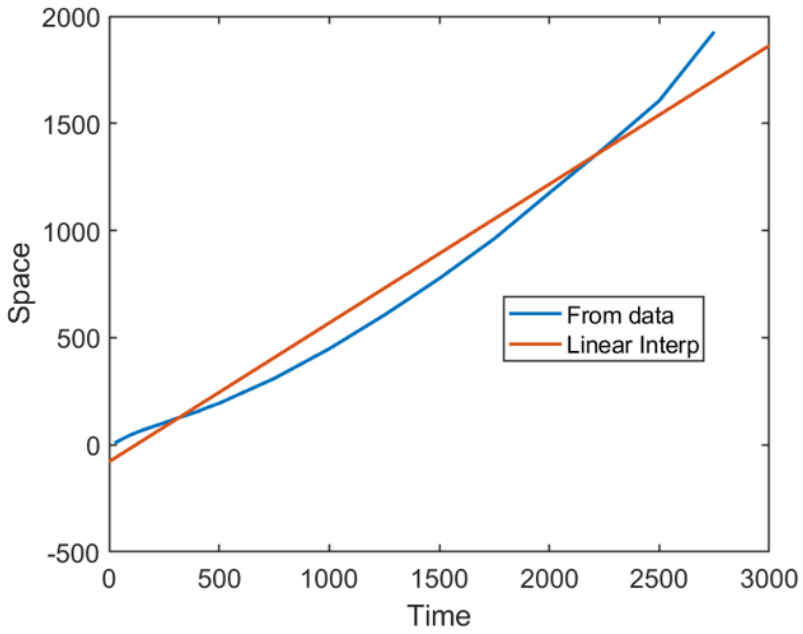

Figure 14: Relation between space and time using δ^*. The blue line represents the result of using function "interp1" and the red one is the linear fit of that result

Using as reference the previous comments on the temporal simulation from this report, it is possible to assume that the temporal case reached the asymptotic state at approximately $t = 1500$. The streamwise domain needed to achieve such state in the spatial simulation is obtained by using the expression 4.11 which predicts an space of roughly $x = 970$ from suction is applied. This result can be checked by looking at the spatial simulation, in which the asymptotic state is reached approximately $x = 750$ after suction. It is true that there is a considerable error but it may be due to the fact that a linear fitting was forced to obtain expression 4.11 while it was much more accurate to use a quadratic fitting.

Despite the possible sources of errors, one thing is clear after the analysis of results, that the boundary layer seems to develop considerably quicker in space than in time,

fact unexpected as the results from Bobke et al.[3] pointed in the opposite direction. However, their relation was obtained through turbulent simulations, that it is why several turbulent cases are explained in the next chapter.

5 | TURBULENT ASBL

The goal of this chapter is to show the results of the performed simulations in a turbulent regime. In order to introduce those result and also to give some context, a previous section of theory is attached where turbulence and its study is briefly explained.

5.1 THEORY

Most flows occurring in nature are turbulent: cumulus clouds, water currents below the surface of the oceans, the flow of water in rivers, the photosphere of the sun or the interstellar gas clouds. In the field of engineering the turbulent flows are also predominant: in combustion engines the combustion process requires a mixing only acquired by turbulent motion, chemical engineers use turbulence to mix new possible compounds and the boundary-layer over a plane wing is turbulent. It can be said that laminar flows are an exception inside fluid dynamics. However, the turbulence, although present everywhere is very difficult to define but there are several characteristics that different turbulent flows always share in common [25]:

IRREGULARITY Turbulent flows are always irregular, non-linear, random and caotic. That fact makes impossible to use a deterministic approach to study turbulence and then an statistic approach is most helpful.

DIFFUSIVITY Property very characteristic of turbulence that employs the energy available on the turbulent flow to spread the homogenisation of the flow by mixing and increasing the convection of mass, momentum and heat. It is the most important characteristic regarding the practical applications.

HIGH REYNOLDS NUMBER When the Reynolds number becomes too high, the smallest instability can lead to the generation of turbulence, turbulent flows always occur at very high Reynolds number where the energy of flow is substantial.

THREE DIMENSIONAL Turbulent flows are characterised by random vorticity fluctuations due to to the rotational character of the flow. These fluctuations are not self-sustained, instead they need a mechanism called vortex stretching that is three-dimensional. In two-dimensional flows, this mechanism is not present and so the vortex fluctuations do not remain and neither the turbulence.

DISSIPATION Turbulence needs a large amount of energy in order to compensate the energy loss due to viscous stresses that converts deformation work into internal energy of the fluid. The turbulent flows are feed by the kinetic energy of the flow itself but when that energy supply is compromised, the turbulence rapidly decay and relaminarise.

FLOW STATE Turbulence is not a feature of the fluid but of the flow itself. The turbulent motion is not influenced by the molecular properties of the fluid.

5.1.1 Mathematical description

The randomness and non-linearity of turbulence make the equations nearly unsolvable, what converts the turbulent theory in one of the principal unsolved physic problems today. The non-linearity character of equations makes that each individual flow pattern has its own characteristics, which are related to the initial and boundary conditions. The flow patterns are very easily influenced by any perturbation. The particular conditions of turbulence makes really complicate to follow the deterministic approach of Navier–Stokes equations. One very used assumption is the asymptotic invariance, that use the property of turbulent flows of having a very high Reynolds number and assumes that it is infinite, leading to an asymptotic state. That assumption simplifies a lot the analysis but is not useful for many studies as for example when the flow is at its transitional state. A much more followed and general approach to treat turbulence is the the use of statistics mechanics, similar to the analysis used in quantum mechanics, as it allows to understand a chaotic system.

The statistic approach requires to use mean variables as well to mean equations. The first step to that is the Reynolds decomposition, which consists on dividing every variable in the Navier-Stokes into a mean and a fluctuation in the following way:

$$u_i = U_i + u_i' \tag{5.1}$$

The U_i is interpreted as time average, defined as:

$$U_i = \lim_{T\to\infty} \frac{1}{T} \int_{t_0}^{t_0+T} u_i \, dt \tag{5.2}$$

Knowing that the average of the fluctuations is null, it is possible to follow a process called equation's filtrate in which the Boundary-Layer equations are subjected to the Reynolds decomposition and consequently leads to a different set of equations with a new unknown, the Reynolds Stress Tensor, $R_{ij} = \overline{u_i' u_j'}$. The new momentum equation:

$$\frac{\partial}{\partial x_j}\left(U_i U_j\right) = -\frac{1}{\rho}\frac{\partial P}{\partial x_i} + \frac{\partial}{\partial x_j}\left(\nu \frac{\partial U_i}{\partial x_j} - \overline{u_i' u_j'}\right) \tag{5.3}$$

The Reynolds stresses are not tensions in practical terms, as they come from the total derivative of the convective part of the equation. They can be considered as the mean effect of the turbulent convection although it is known that they have diffusive behaviour similar to molecular viscosity. As a tensor it has several components:

$$R_{ij} = \begin{bmatrix} \overline{u'^2} & \overline{u'v'} & \overline{u'w'} \\ \overline{u'v'} & \overline{v'^2} & \overline{v'w'} \\ \overline{u'w'} & \overline{v'w'} & \overline{w'^2} \end{bmatrix} \tag{5.4}$$

From the Reynolds' decomposition there are other quantities that can be derived that help to describe and quantify the turbulence as the turbulent intensity and the kinetic energy turbulent:

$$\textbf{Turbulence intensity} \qquad I = \frac{u'}{U} \tag{5.5}$$

$$\textbf{Turbulence kinetic energy} \qquad k = \frac{1}{2}\overline{u_i' u_i'} \tag{5.6}$$

For the definition of the turbulent intensity the concept of root-mean-squared (RMS) was used for the fluctuations. Therefore, u' is defined as $u' = \sqrt{\frac{1}{3}(u'^2 + v'^2 + w'^2)}$. On the other side U is the mean velocity which is defined as $\sqrt{U^2 + V^2 + W^2}$.

It is important to say that the inclusion of the Reynolds stress tensor lead to a closure problem as it introduces more unknowns. This needs to be solved figuring out new equations for the fluctuations. Those new equations can use for example the kinetic energy or the intensity. They are also called models of turbulence as they help to describe turbulence which basically consists on using a RANS approach. Some of the most famous models are: Spallart-Almaras, $k-\epsilon$, $k-\omega$, etc. However, in this project DNS is employed so the turbulence does not need to be modelled.

5.1.2 Viscous scaling

The shear stress in the boundary layer has two different components, the viscous term as before but also a factor of the Reynolds stress. It is expressed as follows:

$$\tau = \rho\nu\frac{\partial U}{\partial y} - \rho\overline{u'v'} \tag{5.7}$$

Close to the wall the convective terms disappear due to the no slip condition, which means that the shear stress and the pressure terms are balanced in the general equation. It becomes clear that the shear stress near the wall has certain relevance so the wall

shear stress, which was previously defined by equation 2.15, is dominated by the viscosity stress. On the contrary, far from the wall, the viscous stresses are always negligible compared with the Reynolds stresses. This fact justifies the fact that it is necessary to have different scales in order to properly analyse both cases, one outer scale that is based on the characteristic lengths of the flow and an inner scale based on the wall shear stress that represent the flow close to the wall.

The friction velocity is the the velocity scale appropriate for close-to-the-wall measurements:

$$u_\tau = \sqrt{\frac{\tau_w}{\rho}} \tag{5.8}$$

Although it seems to be a weird definition the units match with the ones of velocity, but it really represents the importance of the wall shear stress. In the same way, the viscous lengthscale is defined:

$$\delta_\nu = \nu\sqrt{\frac{\rho}{\tau_w}} = \frac{\nu}{u_\tau} \tag{5.9}$$

If a Reynolds number were defined using viscous velocity and lengthscale it would be equal to the unity. For this reason the friction Reynolds number was defined:

$$Re_\tau = \frac{u_\tau \delta}{\nu} = \frac{\delta}{\delta_\nu} \tag{5.10}$$

Using the viscous lengthscales it is now possible to rescale the y direction and the velocity:

$$y^+ = \frac{y}{\delta_\nu} = \frac{u_\tau y}{\nu} \qquad u^+ = \frac{u}{u_\tau} \tag{5.11}$$

Looking at the definition of y^+ it is possible to realise that it is very similar to the friction Reynolds number so it is valid to use it as a measure of the relative importance of the viscous stress and the turbulent ones.

This new scale leads to define new layers or regions close to the wall according to the behaviour of the flow looking at its velocity profile. There exist a region called the viscous wall region where the effects of molecular viscosity are directly influencing the shear stress, approximately at $y^+ < 50$, while in the outer region the effect of viscosity is negligible, $y^+ > 50$. On the contrary, there is also an inner region, $y/\delta < 0.1$, which includes the viscous wall region and also the log-law region. Inside the viscous wall region there exist a zone called viscous sublayer where the Reynolds stresses are negligible compared to the viscous ones and it can be considered that the relation $u^+ = y^+$ is universal, valid for $y^+ < 5$. All of this can be much clearer explained using a table from the book(add reference) and also an oversimplified graph of the velocity profile in viscous units:

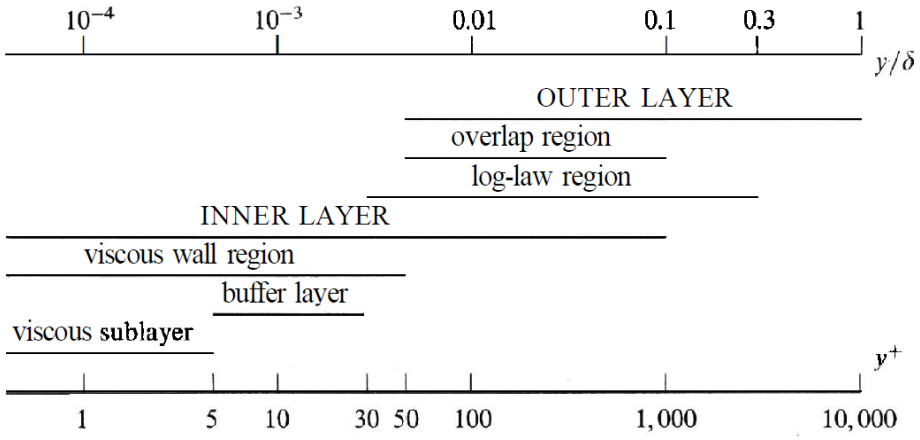

Figure 15: Table summarizing the most relevant regions in the turbulent velocity profile [5]

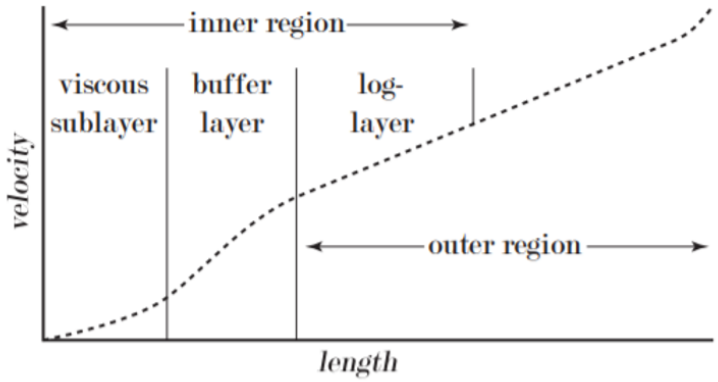

Figure 16: Turbulent velocity profile in wall units and logarithmic x axis [6]

It is clear that figure 16 is a simplification of the reality but it can help to have a first view and know what to possibly expect. Depending on which flow type is being studied, the velocity profile will have some differences and also with different Reynolds number.

5.1.3 Turbulent ASBL

The existence of the asymptotic state of the suction boundary layer in laminar regime was proven to exist a long time ago by Kay in 1948 [11] experimentally and by Meredith and Griffith in 1936 [10] theoretically. It has also been proven to exist by the simulations carried out in this studied which results are exposed in the previous chapter. However, the existence of the asymptotic state in turbulent regime does not raise

the same level of agreement as the laminar case, although many experimental and numerical studies have been done about the topic. Finding an asymptotic state for any value of suction rate has been questioned, firstly Dutton [12] claimed that the asymptotic state can only be reached with a single value of suction rate. Years after that, Tennekes [26] suggested that there exist a threshold value of suction rate under which the asymptotic state is not reached. On the other hand, the mentioned papers of Tennekes and Dutton also stated that for too high suction rates, the boundary layer would relaminarise. That critical suction rate was recently obtained by Khapko et al. [26] in a numerical and was $\Gamma_{crit} \approx 0.0037$. Finally, a recent large-eddy simulation study by Bobke et al. [3] claims that it is impossible to obtain a TASBL experimentally in a realizable facility due to the extremely large length of the streamwise suction direction required. However, an experimental studied made by Ferro et al. [14] claims the opposite, that an asymptotic turbulent state is possible to obtain in a realizable facility if the suction is applied to the already turbulent Blasius boundary layer when the thickness is close to the asymptotic one. The main point of disagreement between those papers is the fact that in the numerical study, the suction is applied on the whole streamwise domain, from a the laminar ASBL and then using a tripping force turbulence is generated while in the experiment the boundary layer is already turbulent when the suction is applied. The final goal of this thesis is to determine which option is correct. In order to do that, the conditions of the Bobke's paper [3] will be reproduce, at least the temporal simulations, while a spatial simulation will be perform using an already turbulent boundary layer before the suction is applied.

Another current point of discussion is about the different scaling laws of the mean velocity profile. For the viscous sublayer there is a general agreement in scaling law, which is defined as:

$$U^+ = \frac{1}{V_0^+}\left(e^{y^+ V_0^+} - 1\right) \tag{5.12}$$

However, for the turbulent layer two different models are proposed. Some authors like Black and Sarnecki, Simpson and Stevenson support the bi-logarithmic law derived from Prandtl's momentum transfer theory. It can be expressed as:

$$\frac{2}{V_0^+}\left(\sqrt{1 + U^+ V_0^+} - 1\right) = \frac{1}{\kappa}\ln y^+ + B \tag{5.13}$$

Although there is not a consensus on which numerical value use for κ and B, there is a general trend that assume that they depend on the suction velocity.

On the other hand, authors like Dutton, Tennekes and recently Bobke et al. [3] believe that exist a logarithmic relation between the streamwise velocity and the wall-normal coordinate as in the case of non-transpired boundary-layers:

$$U^+ = A \ln y^+ + B \tag{5.14}$$

5.2 TEMPORAL SIMULATIONS

With the background provided by the last section where a general explanation of what turbulence is and how to deal with it, it is possible to analyse the turbulent simulations. In particular, this section is going to show the results of the temporal simulations performed with SIMSON. The main goal is to observe how the turbulent suction boundary layer evolves with time. However, as two simulations with different box dimension were run, it is also possible to observe the effect of the box size on the turbulent structures development. The simulations are a replication of the ones performed at Bobke et al. [3], so the fact of obtaining results close to them would be a good sign. Due to the fact that DNS is being used, only the smallest set-ups from Bobke et al. [3] were selected. It is important to comment that in that paper DNS was not used but LES which reduced the computational work.

One great difference compared to the laminar cases is that the spanwise direction is now relevant, in fact, as Bobke et al. [3] says in the paper, it is very important. They proved that by reducing the size of the spanwise direction, many turbulent structures were not able to appear and so the boundary layer was unable to completely develop. Due to this fact, the discretisation in that direction can no longer be reduced to only one point. This convert the simulations into 3-D, which is mandatory to simulate turbulent flows as it is a fundamental property of turbulence. In addition to this, the initial condition, instead of being a Blasius profile, it is the laminar ASBL profile obtained before. In order to obtain the turbulence, a nearly negligible disturbance at $t = 0$ is added to the flow and it is progressively growing with time until a certain level of turbulence is reached.

Name	Re_{δ^*}	Domain Size XYZ	Resolution	δ_{99}	Re_τ
turb333a	333	$100 \times 300 \times 50$	$32 \times 201 \times 32$	73	146
turb333b	333	$200 \times 300 \times 100$	$64 \times 201 \times 64$	101	180

Table 5.1: Set-up data for the temporal turbulent simulation of ASBL. All the data summarized in this tables has been scaled with the initial displacement thickness.

The table above properly summarizes the information about the simulations. The first difference with the laminar cases is the fact of using a Reynolds number of 333 instead of the previously used 450. The reason to this change is to obtain more resemblance with the Bobke's paper, although it is true that in order to make a reasonable comparison with the laminar and the following spatial case this simulations will need to be repeated using $Re = 450$. On the other hand, the domain size as well as the discretisation is the same as in the Bobke's paper for the two smallest cases. The values

of the boundary layer thickness and the friction Reynolds number were obtained after performing the simulation although it is convenient to show them in the table, as they lead to a grid resolution in wall units of $\Delta x^+ = 58$ and $\Delta z^+ = 29$. That resolution is very close to the one used in the paper and shows the relevance of the spanwise direction, where more resolution is needed to capture all the structures.

It is also possible to observe that the boundary-layer thickness, δ_{99}, considerably increase from case turb333a to turb333b as direct consequence of the increase in the spanwise direction. That implies the boundary layer in the second case is more developed than in the first case so it will be a better option to study. Nevertheless, in the paper mentioned before, it is also said that for the size used in the case turb333b, the boundary layer is still not completely developed and that it needs, at least, to double the size of the box in the horizontal plane in order to completely develop the boundary layer.

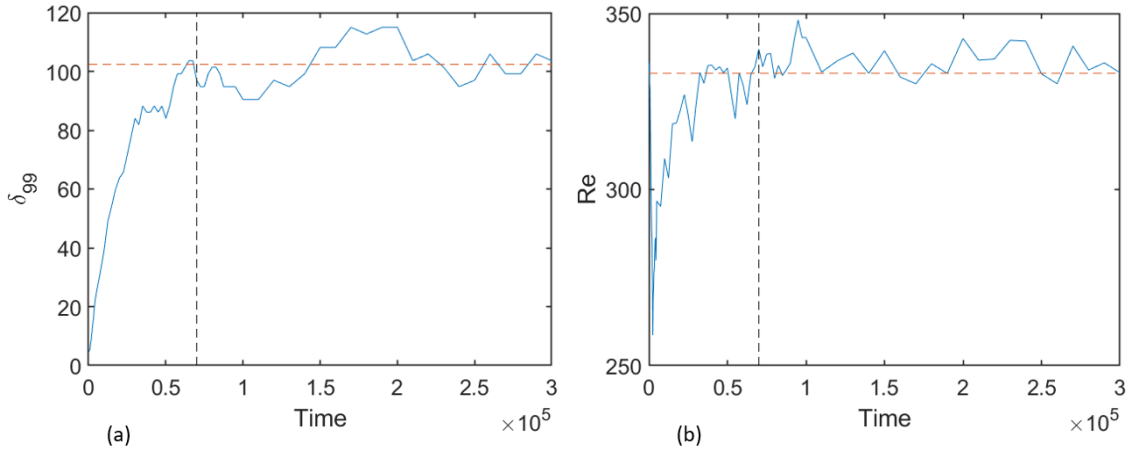

Figure 17: (a) Boundary Layer thickness evolution with time. (b) Reynolds number obtained using friction velocity evolution with time.

Contrary to the laminar case where the boundary layer converged to a previously known state deduced analytically, in the turbulent case there is no known state into which the boundary layer must converge. For this reason, it is complicated to asses if the TASBL, the asymptotic state, is reached. In Bobke's paper [3], it is concluded that the required time to reach the asymptotic state is 2.8×10^5 convective time units. However, that result correspond to domain size of $800 \times 300 \times 400$, which is 4 times bigger than the example case turb333b and consequently requires more time, as the boundary layer is completely developed. As the employed domain size is much smaller than that, it is expected that the time required to obtain the asymptotic state is also smaller. That it is why the simulations were ran until 3×10^5 convective times units and the TASBL was obtained before, at 7×10^4. That value correspond with the point on which

the values of boundary-layer thickness start to stabilize and the Reynolds number too. It also results from assuming a direct relation between the time until asymptotic state and domain size and, the domain is 4 times bigger than the one used here it would also be the time.

On figure 17 it is possible to see how the time has a direct impact on the boundary layer. Those two graphs allow to have an idea of the convergence towards the asymptotic state. In the first one, figure (a) shows the boundary-layer thickness which is obviously growing with time until the asymptotic state is reached, when it just stabilizes and keeps constant. On the other graph, the Reynolds number evolution is showed although it is based on the friction velocity, u_τ, which is obtained using the expression 4.8. In the beginning the Reynolds number is just the initial value, 333, but just after that, as the initial conditions are laminar, no turbulence appear and so the friction is very low. For this reason the Reynolds number directly falls and as the turbulence is generated, there is more friction, and so the Reynolds number rapidly rise until it is stabilize around the value of Reynolds number derived from the suction rate, $Re = \frac{1}{V_0}$ from equation 4.6.

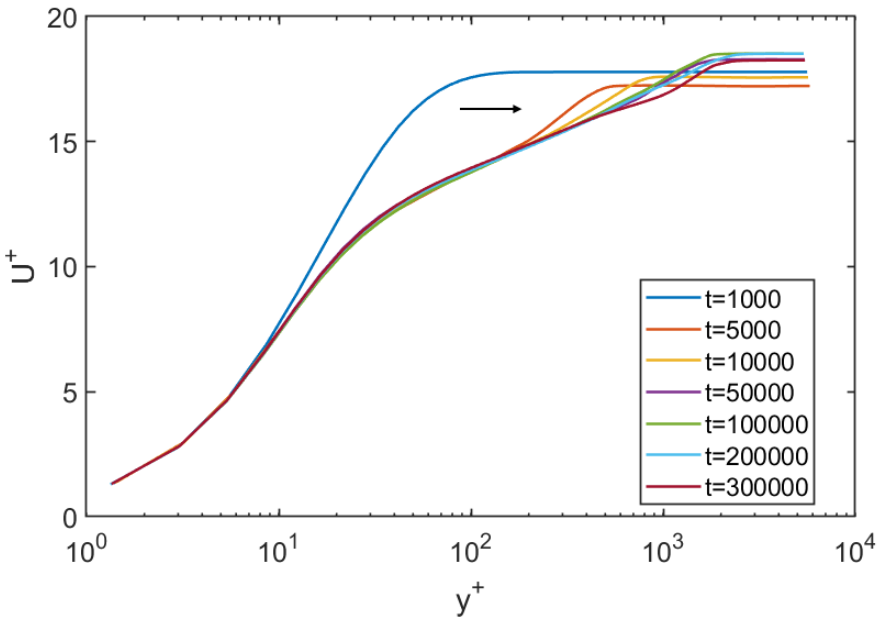

Figure 18: Turbulent velocity profile evolution with time

The results shown until now prove that the TASBL is reached for small spanwise domains and supports the thesis of Bobke's paper [3]. However, there are some disagreements with that paper concerning the values of the boundary-layer thickness and the friction Reynolds number. That it is mainly caused to the fact that, in the present simulations the same grid spacing as Bobke et al. [3] has been used although in their

case the simulations were performed using LES while here DNS has been used. It is believed that the use of that grid without a model of the smallest turbulence caused the slight disagreement in the results.

In figure 18 the mean velocity profile scaled into wall units is represented for different moments in time. It allows to observe the influence of time in the development of the boundary layer. After the first instants where the laminar conditions predominated as the turbulence was not completely developed, the mean velocity profile had a non-recognizable shape. Rapidly, as the turbulence grew, the mean velocity profile adapted the previously mentioned log-law behaviour. Once that is reached, the development is much slower with changes mainly on the wake which is is being reduced. The wake correspond to the last slope change before the mean velocity reaches the corresponding value in the mean flow, out of the boundary-layer. As that slope becomes less rough, the wake strength is diminished. That behaviour is linked to the development of big turbulent structures on the outer zone. When the asymptotic state is reached the variations in the wake become negligible although there is still a considerable slope due to the fact that not all the big structures were allowed to grow as a consequence of the small spanwise dimensions.

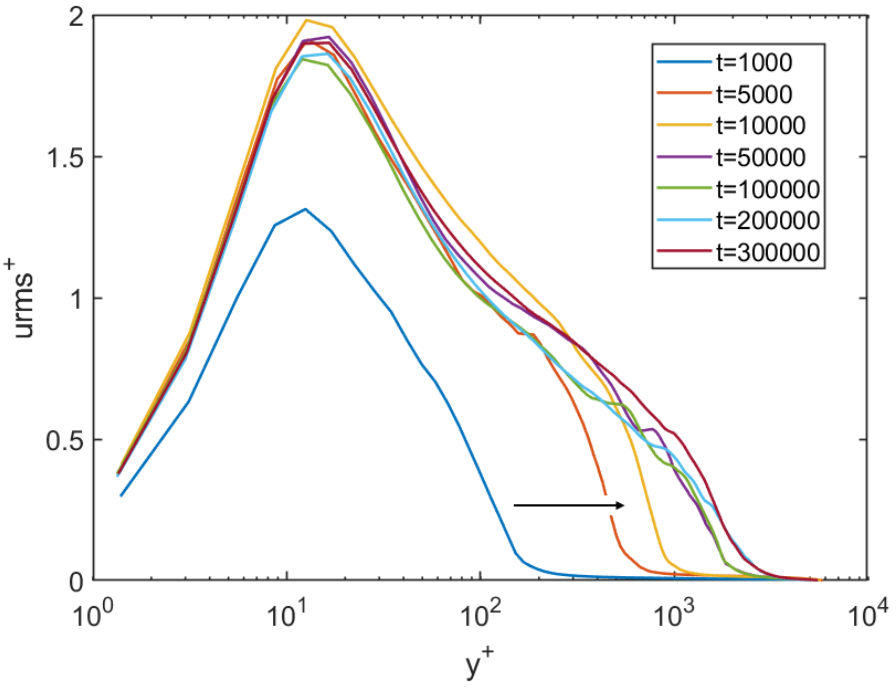

Figure 19: Streamwise velocity fluctuations evolution with time

Another important statistic to look at is the streamwise fluctuations, which are analysed using the root mean square method, then they can me called uRMS. Figure 19

shows the streamwise fluctuations profile and how it changes with time. It is possible to appreciate that the fluctuations become more intense with time, fact that is very noticeable on the outer region where the transition towards the asymptotic state is more obvious. From both pictures can be extracted that with running time, bigger structures grow in the outer region and further they developed. Those structures are diffusing towards the free-stream region and with it, the boundary-layer thickness increases and the wake region is diminished. This growth is stopped when the asymptotic state is reached, but on the examples showed here it is not completely possible to say that such state is reached as the structures are not allowed to grow in the spanwise direction.

Finally, the effect of the spanwise domain is going to be demonstrated. In order to do so, figure 20 shows the streamwise turbulent structures in both cases, turb333a and turb333b. It is possible to observe that with a bigger spanwise box size, the structures becomes bigger and appear higher in the graph. The red line indicates the boundary layer thickness which is determined by the absence of any more turbulence. The relevance of the spanwise dimension is a prove of the vortex stretching mechanism of turbulence which generate the structures examined here.

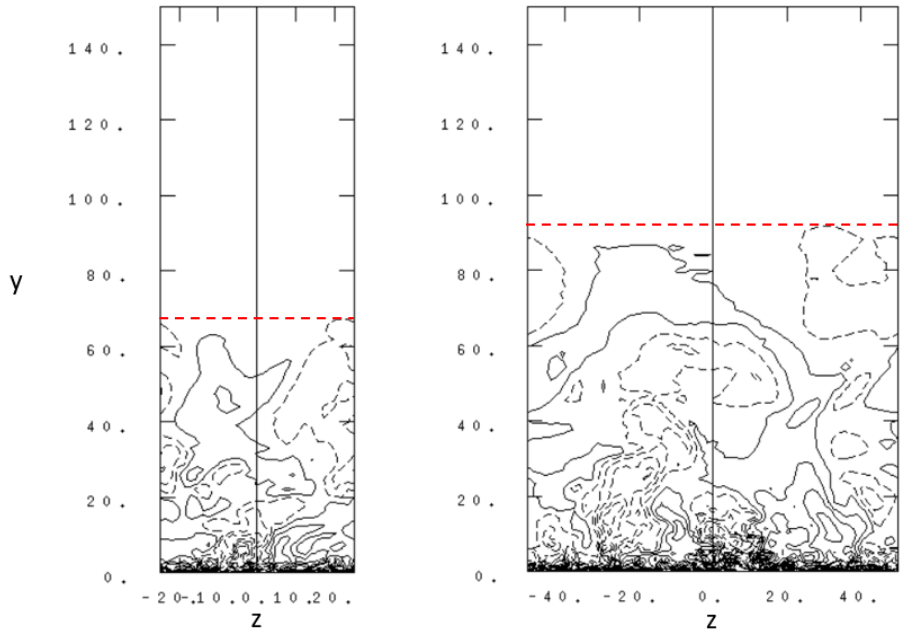

Figure 20: YZ planes of both temporal turbulent simulations. The red-dashed line represents the boundary-layer thickness.

5.3 SPATIAL EVOLUTION

Similarly to what was done in the laminar cases, to the temporal case above it must be added an analogous spatial simulation. This simulation intends to show how the boundary layer with suction evolves on the streamwise direction and it will try to establish a relation between space and time for TASBL. The main parameters of the simulation are summarized on the following table, just as in the temporal case:

Name	Re_{δ^*}	Domain Size XYZ	Resolution	δ_{99}	Re_τ
turb333s	450	$3000 \times 150 \times 50$	$1024 \times 121 \times 32$	32	80

Table 5.2: Set-up data for the spatial turbulent simulation of ASBL. All the data summarized in this tables has been scaled with the initial displacement thickness.

Regarding the domain and the resolution of this simulation, it is practically identical to the spatial simulation in Bobke et al. [3], except for the streamwise coordinate. It has been cut down to the half because the computational cost would be too high to simulate it in the local computers of the department. The simulation had already taken almost two days to finish so doubling the streamwise domain was not convenient. Also due to that reason, instead of using DNS to simulate, the same LES model as in Bobke et al. [3] was employed in order to avoid resolving the smallest scales and saving computational effort. As in the laminar case the suction is applied at $x = 500$ at with the same suction rate 0.003. The spanwise domain is quite small compared to the biggest temporal cases in Bobke et al. [3] so the results obtained are probably not really completly developed as it was already proven that the spanwise domain directly affects the boundary-layer thickness.

The initial conditions for this simulation are different than the ones of the temporal simulation. While in the temporal case, the initial flow field consisted on the laminar ASBL with a perturbation that grew with time and generated turbulence, for this case the initial flow field consist on Blasius boundary layer which is initially laminar. In order to achieve the turbulence, “tripping" was introduced before the suction was applied achieving a Blasius turbulent boundary layer on which suction was applied. That set-up has the advantage that it is much easier to achieve in a wind tunnel experiment and so matches properly with the conditions established by the paper of Ferro et al. [14].

Despite the fact that in the temporal simulation δ_{99} was very useful to detect if the asymptotic state was reached, for this simulation it was not so useful. By looking at figure 21 (a) it is not possible to say that the asymptotic state is achieved as it seems that the thickness would continue to grow for a while. In order to check that possibility, the displacement thickness has been also plotted in figure 21 (b). In that graph, it is

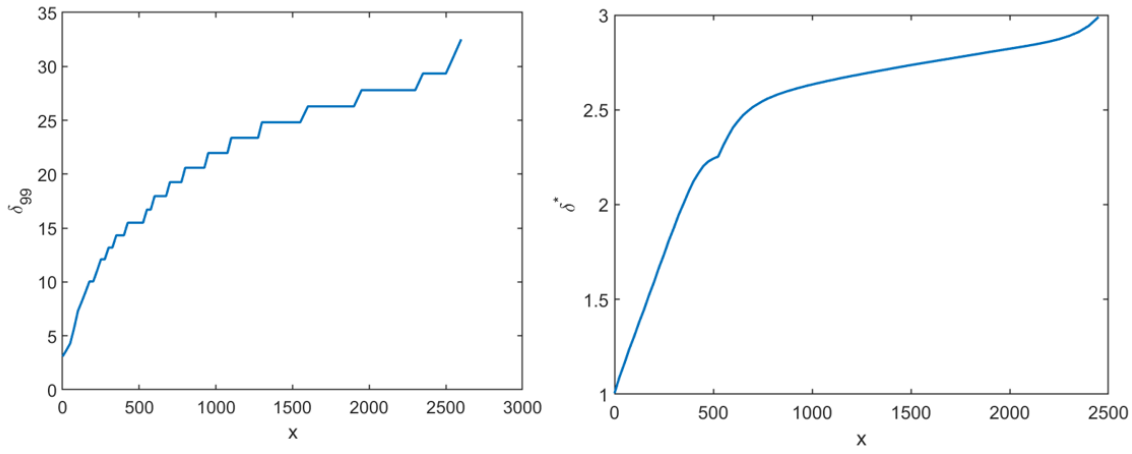

Figure 21: (a) Evolution of δ_{99} on the streamwise coordinate. (b) Evolution of δ^* on the streamwise coordinate.

clear that there exists a transition at $x = 500$ from Blasius to suction as the change in the slope is considerably abrupt. In addition to that, it is again impossible to say that the boundary layer will stop growing. This effect is probably caused to the fact that the streamwise domain may be insufficient for completely reach the asymptotic state. However, as the ultimate goal is to find a tendency between time and space the simulation can be admitted as valid.

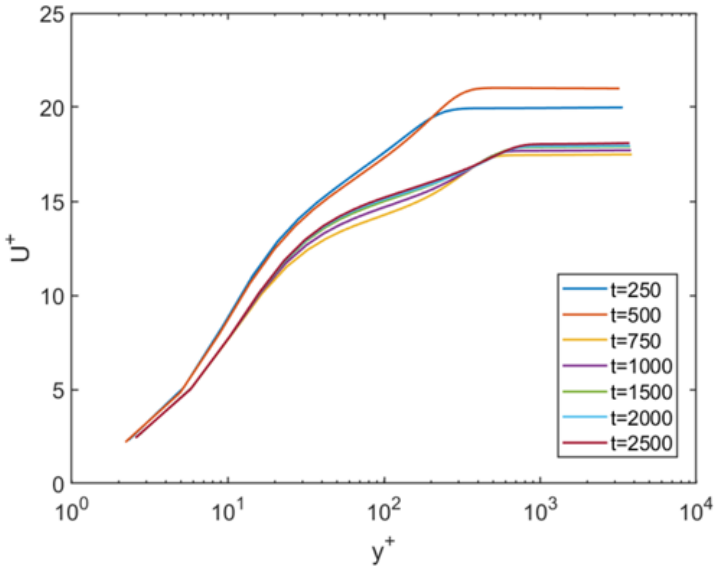

Figure 22: Mean streamwise velocity profiles of the spatial simulation

In figure 22 two very different types of profiles appear,the first two corresponding to the first points on the the streamwise domain which are Blasius type boundary layer and the rest of profiles on which suction is already applied. The two Blasius profiles appear much upper on the graph than the suction ones and show a much more noticeable wake, probably due to the fact that in the first stages the turbulence is still developing. Regarding the profiles in which suction is already applied, it is possible to see how the wake is slowly reducing and so the slope of the curve is less marked. However, this graph is, in a way, contradictory with figure 21 because here it seems that the velocity profile is collapsing and that any possible change would not be very remarkable. To support that idea, the value of the boundary layer thickness, δ_{99}, is very close to the ones of the spatial simulation in Bobke et al. [3]

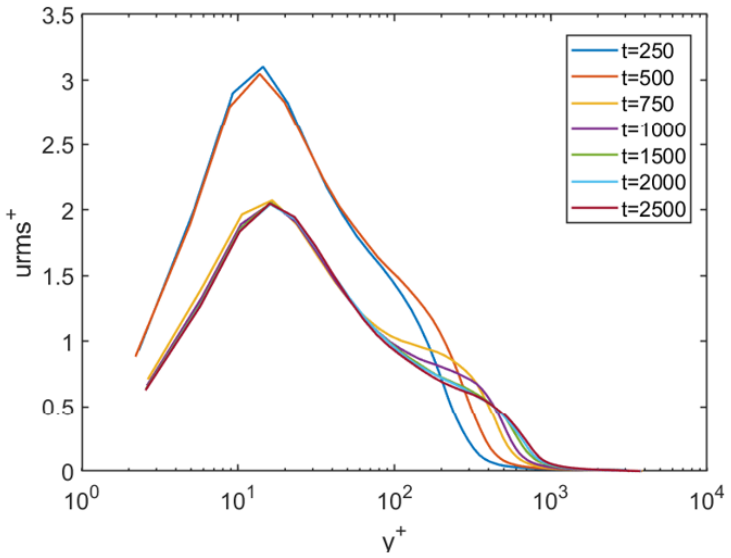

Figure 23: Root-mean-square of the streamwise velocity fluctuations

Figure 23 also supports that the boundary layer is near of reaching the asymptotic state, as the differences in the wake region are getting smaller. There is also a great difference with the Blasius profiles, they seem to achieve much higher level of fluctuations, or at least the peak is higher than for the profiles with suction. The fact that the wake region in the fluctuations profiles indicates, as in the temporal simulations, that the bigger turbulent structures are being developed. As due to short spanwise domain the turbulent structures are not allow to grow as much as they can, it is expected that, as much as the streamwise domain is increased, if the spanwise coordinate is not increased together, wake region will not disappear.

Finally, in order to actually visualize what it is happening in the boundary layer figure 24 is attached. Thanks to that it is possible to observe how the turbulent structures appear in the boundary layer and how the bigger ones are located on top of it

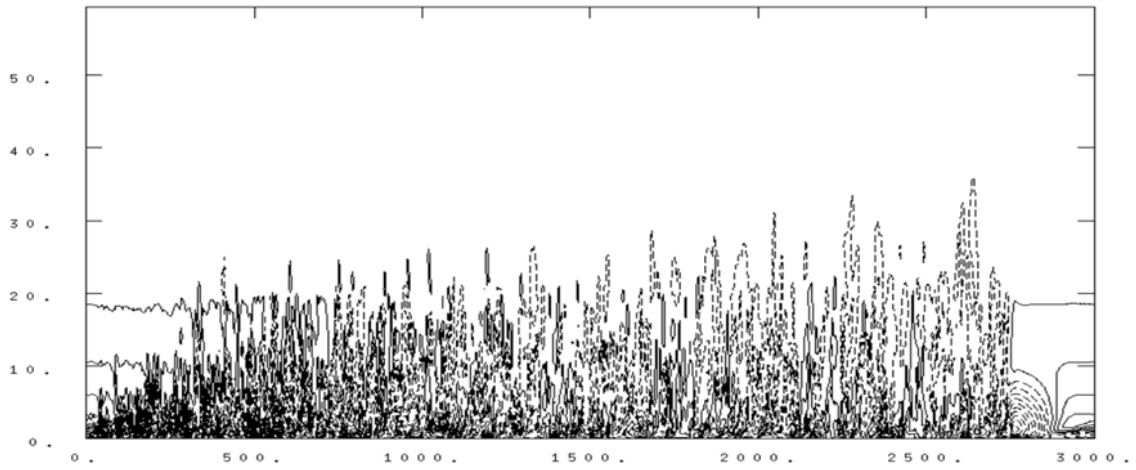

Figure 24: XY plane of the spatial simulation showing the turbulent structures

while the smaller ones are very close to the wall. In addition to that, as the boundary layer goes further in x the structures near to wall also get bigger than the ones in the beginning of the domain. It is also possible to visualize the effect of the fringe region, which is located at the end of the domain and disturbs the flow considerably to fulfil periodic boundary conditions.

5.4 COMPARISON

Following the same procedure that was used for the laminar cases comparison, this section is going to show the relation between time and space using both turbulent simulations. However, in contrast with the laminar simulations, the initial conditions of the turbulent ones are not really analogous because the temporal case use a laminar ASBL with a perturbation growing in time and suction applied all along the domain while the turbulent case employs a Blasius boundary layer in which turbulence is induced by tripping and after $x = 500$ suction is applied. Those differences in the initial conditions do not favour the accuracy of the comparison and so then the results of it must be taken with caution. To reinforce that, the Reynolds number used in the simulations is different.

The parameter used this time for the comparison is the boundary-layer thickness δ_{99} as for the turbulent simulations its evolution is significant. In addition to that, it is the parameter used in the paper by Bobke et al. [3] which is being used as reference. An important comment about the comparison is that, instead of using the bigger temporal simulation which was analysed in the section about the temporal case, it has been used the smaller case `turb333a` because its spanwise domain is the same as the one of the

spatial simulation. This decision helps to improve the comparability of the simulations although it is also true that with such small domain in z coordinate it is not possible to assume that the boundary layer is completely developed and then so the conclusions are subjected to possible improvements.

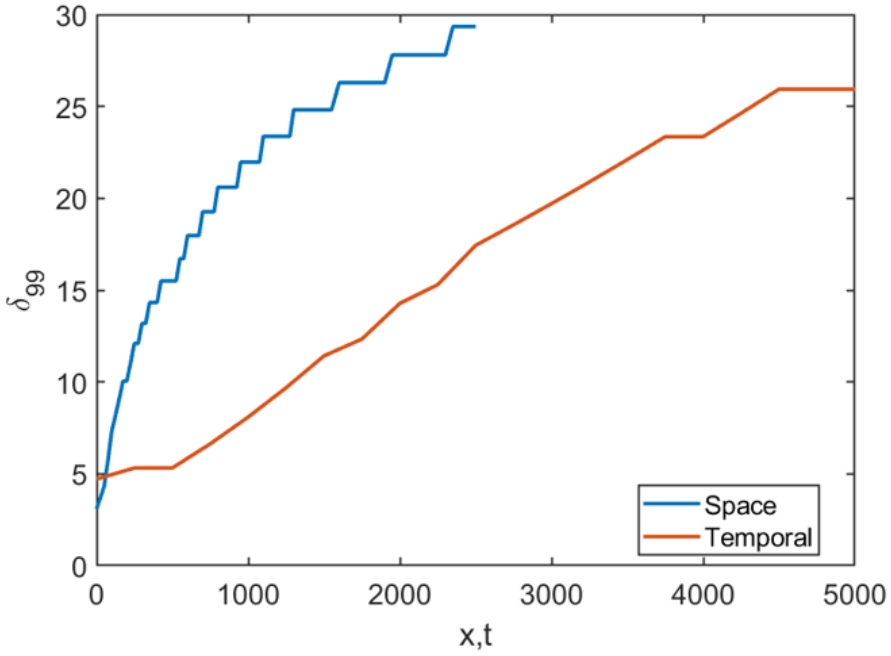

Figure 25: Comparison of boundary-layer thickness δ_{99} between spatial and temporal simulations.

In figure 25 it is possible to observe a similar trend to the laminar case, the boundary layer seems to develop at a much higher rate in space than in time. While the trend of the temporal simulation can be identified as close to linear, the spatial one is much closer to an exponential growth. As in the laminar case, it is necessary to extract a quantitative parameter that helps to establish how much faster is the developed in space than in time. The method to obtain it is the same, using the MATLAB functions in order to find a relation between space and time and then use a linear fitting to use its slope as the parameter desired.

Figure 26 represents the process just explained. As in the laminar case, the direct relation of space and time seems to have a quadratic shape instead of linear but in order to find the simplest relation as possible a linear fitting is performed resulting on the red line. This forcing into the linear fit is, together with the differences of

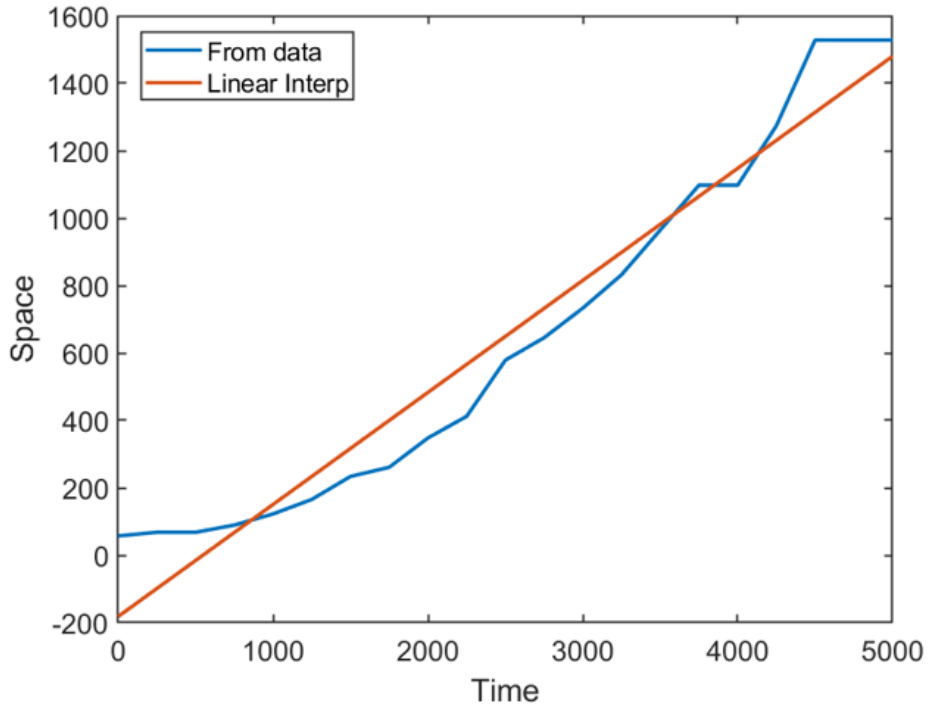

Figure 26: Relation between space and time using δ_{99}. The blue line represents the result of using function "interp1" and the red one is the linear fit of that result

the initials conditions, a source of error. Finally, using the slope of the linear fit, the velocity that relates space and time is found:

$$u_T = \frac{x}{t} \approx 0.33 \tag{5.15}$$

The result is surprising, although it follows the same line as the laminar case, because it contradicts what was said in the paper Bobke et al. [3] where it was considered that the boundary layer developed faster in time than in space obtaining a relation of $u_T = \frac{x}{t} \approx 1.3$. It is important to remember that in that paper, the spatial simulation was different from the one performed for this project. The suction was applied from the beginning of the domain and the initial flow is a Blasius boundary layer which is tripped at the start of the domain so the turbulence is generated when the suction is already applied. Then is not very clear yet if the initial conditions are really comparable. That it is why the results obtained here must be taken with caution as further research and much more detailed simulations are required to confirm these results. A possible cause of the different behaviour between the paper by Bobke et al. [3] and the present simulations is that in their simulations the turbulence is from the beginning restricted by the suction which acts delaying the growth of the turbulent structures.

On the other hand, the spatial simulation done for the thesis allow the turbulence to grow for a while without the effect of suction.

Using the relation between space and time obtained here and the approximated time required to achieve the asymptotic state of the bigger temporal case, turb333b, studied before it is possible to estimate how long the streamwise domain should be in order to reach the TASBL. That simulation reached the asymptotic at approximately $t = 7 \times 10^4$ which applying the relation y_T would require an streamwise domain of at least $x = 23100$ units. At this point it is crucial to remember that lengths are all scaled using the initial displacement thickness δ_0^*. Assuming that the initial displacement thickness is about 1 millimetre which is the assumption made in the paper by Bobke et al. [3], the length required in a real facility would of 23 meters approximately. However, as it was mentioned before, the temporal simulation used for obtained that distance has an insufficient spanwise domain so the boundary layer was not completely developed so that length would not be sufficient either. In the work by Bobke et al. [3] it was proven that the required spanwise domain in order to reach a completely developed TASBL was of $L_z = 400$, which is 4 times bigger than the one used in temporal simulation used as example. Due to that factor of 4 the required time to reach the asymptotic state is also considered to be 4 times higher and then the length required also needs to be longer, so finally the streamwise domain in a real facility to obtain a full TASBL would be:

$$L_x \approx 92m \tag{5.16}$$

This result would require an extremely large wind-tunnel facility in order to actually observe a turbulent asymptotic suction boundary-layer. This would also imply that it might be helpful to re-evaluate some experimental studies, such as the ones by Ferro et al. [14]. The results are then closer to the findings in the work by Bobke et al. [3], in which it is stated that it is not really possible to obtain the TASBL in realizable facility. Nevertheless, their estimated required streamwise length is more than three times longer than the estimation made here, mainly due to the fact that, in this thesis everything seems to point that the boundary layer develops faster in space than in time. However, the results of this thesis are not definitive and so caution must be taken when the results here are interpreted as they require further research.

6 CONCLUSION

In order to conclude the report is it convenient to summarize all the outcomes of the work done. That is the purpose of this section, where the most important conclusions extracted from the research are going to be clearly stated and briefly re-explained to achieve a global point of view.

Regarding the laminar simulations, the most important conclusion extracted is that the asymptotic state of the suction boundary layer is achieved faster in the spatial simulations than in the temporal ones. This means that the boundary layer is developing faster in space than in time, a fact that was surprising after the findings by Bobke et al. [3]. Although there may be inaccuracies mainly due to the linear interpolation, the comparison was quite solid since the initial conditions matched properly. In addition, the estimated streamwise length required to reach the asymptotic state was calculated to be around 1 meter.

Regarding the turbulent temporal simulations the most remarkable outcome, may be the similar results obtained compared with Bobke et al. [3] despite the using DNS instead LES with the same grid. It was also proven the great influence of the spanwise dimension of the computational box.

The most important outcome of the thesis is clearly the relation between space and time for the turbulent simulations. That relation helps to predict that the required length to obtain the asymptotic state in the turbulent suction boundary layer would be of 92 meters, so it would require an immense wind tunnel. This result contradicts previous experimental and computational papers (Ferro et al. [14] and Bobke et al. [3]) but it is more in agreement with the second paper in the way that it would be very difficult to achieve the TASBL in an experiment. Nevertheless, this last conclusion is subjected to further and much more detailed research as there are many sources of errors in the comparison made between spatial and temporal simulations.

In the near future, in order to improve the research made here, more simulations and much accurate ones are required. It would be very convenient to run a temporal simulation with already turbulent initial conditions in order to recreate better the conditions of the spatial simulation. It would also be very useful to run an spatial simulation with an adequate spanwise domain and a longer streamwise one, in that way a completely developed TASBL may be achieved but the computational cost would be very large.

BIBLIOGRAPHY

[1] H. Schlichting and K. Gersten. *Boundary-layer theory*. Berlin Heidelberg: Springer-Verlag, 9 edition, 2017.

[2] R.L. Panton. *Incompressible Flows*. John Wiley and Sons, 4 edition, 2013.

[3] R. Örlü A. Bobke and P. Schlatter. Simulations of turbulent asymptotic suction boundary layers. *Journal of Turbulence*, 17(2):157–180, 2016.

[4] M.Lee and R. Moser. Direct numerical simulation of turbulent channel flow up to $Re_\tau \approx 5200$. *J. Fluid Mech.*, 774:395–415, 2015.

[5] S.B. Pope. *Turbulent flows*. Cambridge University Press, 1 edition, 2000.

[6] J. Malmberg. *Improving Aerodynamic Performance of a Truck: a Numerical Based Analysis*. Master's thesis, KTH Mechanics Department, 2015.

[7] M Jahanmiri. Aircraft Drag Reduction: An Overview, 2011.

[8] B.J. McKeon. Controlling Turbulence. *Science*, 327:1462–1463, 2010.

[9] L. Prandtl. Über Flüssigkeitsbewegung bei sehr kleiner Reibung. *Verhandl III. Int Math Kongr.*, pages 484–491, 1904.

[10] A.A. Griffith and F.W. Meredith. The possible improvement in aircraft performance due to the use of boundary layer suction. Technical Report E3501, Royal Aircraft Establishment, 1936.

[11] J.M. Kay. Boundary-layer flow along a flat plate with uniform suction. Technical report, Cambridge, UK: HM Stationery Office, 1948.

[12] R.A. Dutton. The effects of distributed suction on the development of turbulent boundary layers. Technical report, Cambridge, UK: HM Stationery Office, 1958.

[13] J.C. Rotta. Control of turbulent boundary layers by uniform injection and suction of fluid. Technical report, Jahrbuch Deutsch Gesellsch Luft Raumfahrt E. V. (DGLR), 1970.

[14] P. Mariani, P. Spalart and W. Kollmann. Direct simulation of a turbulent boundary layer with suction. In *So RMC, Speziale CG, Launder BE, editors. Near-wall turbulent flows*, pages 347–356. Elsevier, 1993.

[15] M. Ferro, B. Fallenius and J. Fransson. On the scaling of turbulent asymptotic suction boundary layers. *Proc. Intern. Symp. on Turbulence and Shear Flow Phenomena (TSFP-10), Chicago, USA, July 6-9*, 2017.

[16] J.D. Anderson Jr., J. Degroote, G. Degrez, E. Dick, R. Grundmann and J. Vierendeels. *Computational Fluid Dynamics: An Introduction*. Springer, 3 edition, 2009.

[17] S.M. Hosseini, R. Vinuesa, P. Schlatter, A. Hanifi and D.S. Henningson. Direct numerical simulation of the ow around a wing section at moderate Reynolds number. *Int. J. Heat Fluid Flow*, 61:117–128, 2016.

[18] R. Vinuesa, S.M. Hosseini, A. Hanifi, D.S. Henningson and P. Schlatter. Pressure-gradient turbulent boundary layers developing around a wing section. *Flow Turbul. Combust.*, 99:613–641, 2017.

[19] R. Vinuesa, P.S. Negi, M. Atzori, A. Hanifi, D. S. Henningson and P. Schlatter. Turbulent boundary layers around wing sections up to $\mathrm{Re}_c = 1,000,000$. *Int. J. Heat Fluid Flow*, 2018.

[20] A. Bobke, R. Vinuesa, R. Örlu and P. Schlatter. History effects and near equilibrium in adverse-pressure-gradient turbulent boundary layers. *J. Fluid Mech.*, 820:667–692, 2017.

[21] A. Lundbach M. Chevalier, P. Schlatter and D.S. Henningson. A pseudospectral solver for incompressible boundary layer. Tech. rep., KTH Mechanics, 2007.

[22] J. Kim, P. Moin and R. Moser. Turbulence statistics in fully developed channel flow at low Reynolds number. *J. Fluid Mech.*, 177:133–166, 1987.

[23] Available database for validation. http://turbulence.ices.utexas.edu/.

[24] R. Vinuesa, C. Prus, P. Schaltter and H.M. Nagib. Convergence of numerical simulations of turbulent wall-bounded flows and mean cross-flow structure of rectangular ducts. *Meccanica*, 51:3025–3042, 2016.

[25] H. Tennekes and J.L. Lumley. *A first course in turbulence*. The MIT Press, 1 edition, 1972.

[26] H. Tennekes. Similarity laws for turbulent boundary layers with suction or injection. *J. Fluid Mech.*, 21:689–703, 1965.